Cell

Identification of Aneuploidy-Tolerating Mutations

Eduardo M. Torres,[1,2] Noah Dephoure,[3] Amudha Panneerselvam,[1] Cheryl M. Tucker,[4] Charles A. Whittaker,[1] Steven P. Gygi,[3] Maitreya J. Dunham,[5] and Angelika Amon[1,2,*]
[1]David H. Koch Institute for Integrative Cancer Research
[2]Howard Hughes Medical Institute
Massachusetts Institute of Technology, Cambridge, MA 02139, USA
[3]Department of Cell Biology, Harvard University Medical School, Boston, MA 02115, USA
[4]Lewis-Sigler Institute, Princeton University, Princeton, NJ 08540, USA
[5]Department of Genome Sciences, University of Washington, Seattle, WA 98195, USA
*Correspondence: angelika@mit.edu
DOI 10.1016/j.cell.2010.08.038

SUMMARY

Aneuploidy causes a proliferative disadvantage in all normal cells analyzed to date, yet this condition is associated with a disease characterized by unabated proliferative potential, cancer. The mechanisms that allow cancer cells to tolerate the adverse effects of aneuploidy are not known. To probe this question, we identified aneuploid yeast strains with improved proliferative abilities. Their molecular characterization revealed strain-specific genetic alterations as well as mutations shared between different aneuploid strains. Among the latter, a loss-of-function mutation in the gene encoding the deubiquitinating enzyme Ubp6 improves growth rates in four different aneuploid yeast strains by attenuating the changes in intracellular protein composition caused by aneuploidy. Our results demonstrate the existence of aneuploidy-tolerating mutations that improve the fitness of multiple different aneuploidies and highlight the importance of ubiquitin-proteasomal degradation in suppressing the adverse effects of aneuploidy.

INTRODUCTION

Aneuploidy, defined as any chromosome number that is not a multiple of the haploid complement, is associated with death and severe developmental abnormalities in all organisms analyzed to date (reviewed in Torres et al., 2008; Williams and Amon, 2009). Aneuploidy is the leading cause of miscarriages and mental retardation in humans and is found in 90% of human cancers (Hassold and Jacobs, 1984; Holland and Cleveland, 2009). Despite the high incidence of aneuploidy in tumors, its role in tumorigenesis remains uncertain (Holland and Cleveland, 2009; Schvartzman et al., 2010).

To shed light on the relationship between aneuploidy and tumorigenesis, we previously determined the effects of aneuploidy on normal cells. Twenty strains of budding yeast, each bearing an extra copy of one or more of almost all of the yeast chromosomes (henceforth disomic yeast strains), display decreased fitness relative to wild-type cells and share traits that are indicative of energy and proteotoxic stress: metabolic alterations, increased sensitivity to conditions that interfere with protein translation, folding, and turnover (Torres et al., 2007), a cell proliferation defect (specifically a G1 delay), and a gene expression signature known as the environmental stress response (Gasch et al., 2000). These shared traits are due to the additional gene products produced from the additional chromosomes. Primary aneuploid mouse cells exhibit similar phenotypes (Williams et al., 2008). On the basis of these findings, we proposed that aneuploidy leads to an "aneuploidy stress response." In this response, cells engage protein degradation and folding pathways in an attempt to correct protein stoichiometry imbalances caused by aneuploidy. This puts a significant burden on these protein quality-control pathways, resulting in increased sensitivity to compounds that interfere with protein degradation and folding. Synthesis and neutralization of the proteins produced from the additional chromosomes also lead to an increased need for energy.

The increased sensitivity of many aneuploid yeast strains to cycloheximide and proteasome inhibitors suggests that ubiquitin-mediated protein degradation is one of the protein quality control pathways as being affected in aneuploid cells. During ubiquitin-mediated protein degradation, multiple ubiquitin molecules are covalently linked to a substrate, which allows recognition by the 26S proteasome (Varshavsky, 2005). Upon recognition, ubiquitin chains are removed, and substrates are fed into the catalytic cavity of the proteasome. Two deubiquitinating enzymes, Rpn11 and Ubp6, remove ubiquitin from substrates (Chernova et al., 2003; Hanna et al., 2003; Verma et al., 2002; Yao and Cohen, 2002). Both of these proteases are associated with the proteasome and are essential for ubiquitin recycling. In the absence of either protein, levels of free ubiquitin rapidly decline as a result of degradation of ubiquitin chains by the proteasome. In addition to a role in ubiquitin recycling, Ubp6 regulates proteasomal degradation. In its absence, proteasomal degradation of several substrates is accelerated (Hanna et al., 2006; Peth et al., 2009). The results described

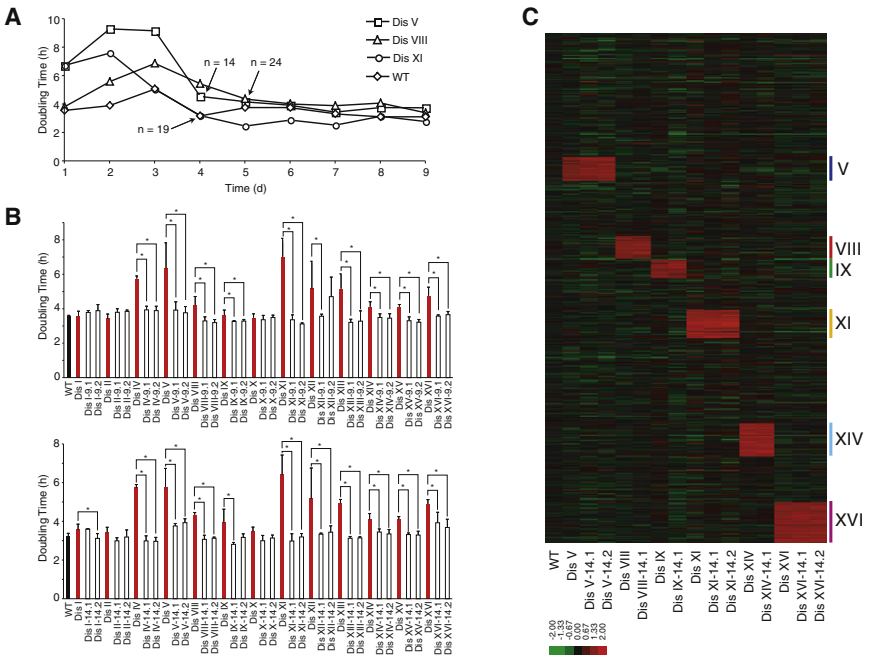

Figure 1. Evolution of Aneuploid Yeast Strains

(A) Doubling times of disome V (open squares), disome VIII (open triangles), disome XI (open circles), and wild-type cultures (open diamonds) were measured at the indicated times. The arrows indicate the generation when growth rates increased.

(B) Doubling times of wild-type cells (black bar), parental disomes (red bars), and evolved isolates (open bars) were determined in −His+G418 medium at room temperature (n = 3, error bars represent ± standard deviation [SD], *p value < 0.01, Student's t test). Nomenclature: The Roman numerals describe the identity of the disomic chromosome. The number after the dash indicates when the clone was isolated (after 9 or 14 days of continuous growth), and the number after the period describes the identity of the clone.

(C) Gene expression analysis of wild-type, parental, and evolved disomic strains grown in batch culture, ordered by chromosome position. Experiments (columns) are ordered by the number of the chromosome that is present in two copies. Data were normalized to account for the extra chromosome present in disomic strains. Upregulated genes are shown in red and downregulated ones in green.

See also Tables S1, S2, and S3 and Figures S1 and S2.

here indicate that Ubp6, through its role in protein degradation control, affects the proliferative abilities of several aneuploid yeast strains.

The consequences of system-wide aneuploidy of only a single chromosome are severe in all organisms analyzed to date (reviewed in Torres et al., 2008). In striking contrast, in most cancer cells, aneuploidy is common, typically involving many chromosomes, but proliferation potential in these cells is high (reviewed in Albertson et al., 2003). To resolve these contradictory observations, we hypothesized that genetic alterations must exist that allow cancer cells to tolerate the adverse effects of aneuploidy. To test this idea, we isolated aneuploid yeast strains with increased growth rates and characterized their genetic alterations. This analysis revealed strain-specific genetic changes and mutations shared between different aneuploid strains. We characterized further one of these shared genetic alterations, a loss-of-function allele in the gene encoding the deubiquitinating enzyme Ubp6. Our studies show that inactivation of *UBP6* improves the proliferation rates of four different disomic yeast strains and suggest a mechanism for this suppression. Deletion of *UBP6* attenuates the effects of aneuploidy on cellular protein composition. Our results demonstrate the existence of aneuploidy-tolerating mechanisms. Enhanced proteasomal degradation appears to be one of them.

RESULTS

Isolation of Aneuploid Yeast Strains with Increased Proliferative Abilities

To identify genetic alterations that suppress the adverse effects of specific aneuploidies or perhaps even multiple different aneuploidies, we sought variants of 13 different disomic yeast strains that proliferate well despite the presence of a disomic chromosome. To isolate variants of disomic yeast strains with decreased doubling time, we used continuous growth under conditions that select for the presence of the disomic chromosome rather than a traditional mutagenesis approach to keep the number of genetic alterations low (Experimental Procedures).

Environmental conditions such as media composition greatly influence the outcome of evolution experiments (Gresham et al., 2008; Zeyl, 2006). Therefore, we initially chose two sets of disomic yeast strains, one that required growth in medium lacking uracil and histidine (−Ura−His medium) to select for the presence of the extra chromosome, and another that required growth in medium lacking histidine and containing the antibiotic G418 (−His+G418 medium). The doubling time of the disomic yeast strains was significantly longer in −His+G418 medium than in −Ura−His medium (data not shown). We suspect that this is due to G418's ability to cause frameshifts during translation (Davies and Davis, 1968; Davies et al., 1964). The increase in frameshifts further enhances the burden on the protein quality-control pathways that help aneuploid cells deal with the proteins produced from the additional chromosomes. The greater difference in doubling time between wild-type and aneuploid cells in −His+G418 medium together with the finding that some disomic strains (e.g., disome V) appeared to lose large parts of the additional chromosome more readily in −Ura−His medium (data not shown) prompted us to perform the selection for disomic strains with increased proliferative rates in −His+G418 medium. Passaging of cells in this medium initially led to an increase in doubling times in many strains (Figure 1A; Table S1 available online). We do not yet understand the molecular basis for this transient slowing of cell proliferation, but we

note that it is reminiscent of the crisis period observed during serial passage of primary mammalian cells in culture (Todaro and Green, 1963). Populations with decreased doubling times emerged shortly thereafter (Table S1).

We isolated single colonies after 9 days (37–66 generations; Table S1) and 14 days (64–105 generations; Table S1). Doubling-time measurements confirmed that 11 out of 13 disomic yeast strains had produced clones with significantly increased proliferation rates (Figure 1B) and changed the cell-cycle distribution to be more similar to that of wild-type cells (i.e., Figure S1A). We predicted that we would obtain two types of suppressor mutations: mutations that improve the growth of disomic yeast strains only in −His+G418 medium in which the cells are coping with the additive stresses of G418 and aneuploidy and are therefore more sensitive to suppressor mutations with milder effects, and mutations that improve proliferation irrespective of which medium cells are cultured in. This appeared to be the case. All evolved isolates obtained from disomes IX, XI, XIII, and XVI (the disomic strains whose proliferation is only minimally affected in YEPD medium to begin with) showed fitness gain only in −His+G418 medium but not in YEPD (Figure S1B). This phenomenon of genomic alterations being condition specific has been observed previously (i.e., Dettman et al., 2007). We conclude that aneuploidy-tolerating mutations exist that are growth condition specific and that improve proliferation more generally.

Evolved Isolates Obtained from Four Disomic Strains Exhibit Gross Chromosomal Rearrangements

To determine the basis for the decrease in doubling time in the evolved disomic strains, we first examined their karyotypes. *C*omparative *g*enome *h*ybridization (CGH) analysis revealed that the overall chromosomal composition was not altered in the majority of disomic strains (Table S2). Thus, the improved growth rates of these isolates must be caused by alterations that are undetectable by CGH analysis.

Descendants of strains disomic for chromosome IV experienced loss of the entire additional chromosome and most diplodized (Table S2). Isolates obtained from strains disomic for chromosome XII, XIV, or XV had lost large parts of one copy of the duplicated chromosome but also carried a duplication of a region of the left arm of chromosome XIII (TEL13L–YML046W; 183 kb, 345 genes; Table S2). It is highly likely that loss of all or part of the chromosome present in two copies is in large part responsible for the increase in proliferation rate seen in the evolved strains, but we speculate that genes exist in region TEL13L–YML046W, whose 2-fold increase in copy number improves proliferation of three different disomic yeast strains.

Truncations of the duplicated chromosome occurred in or next to Ty elements, retrotransposons that are scattered throughout the yeast genome. This correlation indicates that homologous recombination between these repeated elements was responsible for the loss of these regions. The ends of regions TEL13L–YML046W were also at or near Ty elements. Given that region TEL13L–YML046W does not carry a centromere but is nevertheless stably inherited, it is highly likely that the duplicated region TEL13L–YML046W represents a translocation caused by Ty element-mediated recombination. Our results indicate that cells carrying an extra chromosome rapidly evolve and acquire genomic alterations. These include point mutations (see below), truncations, amplifications, and whole-genome duplications.

Expression of the Genes Encoded by the Duplicated Chromosomes Is Not Attenuated in the Evolved Isolates

We showed previously that the majority of genes present on the disomic chromosome are expressed according to gene copy number exhibiting an average increase in gene expression of approximately 1.82-fold (Torres et al., 2007). Downregulation of gene expression of the disomic chromosome, like loss of large parts of the additional chromosome, could lead to increased proliferation rates. Gene expression analysis of the evolved strains that retained both copies of the disomic chromosome showed that gene expression of the chromosome present at two copies was not attenuated even though proliferation rates were increased (Figure 1C). Average expression of genes present on the disomic chromosome was increased an average of 1.84-fold compared to the rest of the genome. Thus, attenuation of gene expression of the disomic chromosome is not responsible for the improved proliferation rates.

Our previous analysis of the disomic strains revealed a transcription profile shared by different disomes (Torres et al., 2007). This aneuploidy signature was only seen under conditions that eliminated the differences in growth rate between aneuploid strains (cells were grown in the chemostat under phosphate-limiting conditions). Gene expression analysis of the evolved isolates grown under these conditions confirmed that global gene expression patterns were maintained, with each evolved strain clustering most closely with its parental disomic strain (Figure S2A). Interestingly, the gene expression patterns of the two evolved disomic strains that we analyzed were more similar to each other than to the parental disomic strain (Figure S2A). This result suggests that the genetic alterations in the different isolates affect the same pathways and lead to a similar transcriptional response in the evolved strains.

To determine whether the evolved strains share a transcriptional profile that is distinct from that shared by the parental strains, we subtracted the original disome expression values from that of the evolved strains. This analysis revealed a common expression pattern among the evolved strains (Figure S2; Table S3). Ion transport, especially iron, and a subset of ribosomal proteins were significantly enriched in the decreased expression cluster (Table S3). Genes with increased expression were enriched for genes involved in amino acid metabolism (p value = 9.69×10^{-20}). This group includes many of the genes responsible for biosynthesis of aromatic amino acids, branched chain amino acids, and arginine (Table S3). The significance of this expression signature is at present unclear, but we speculate that increased protein synthesis as a result of the presence of an additional chromosome (see below) may bring about the need for increasing production of amino acids. Strain-specific expression changes also occurred. For example, a small group of genes increased in expression in both isolates from disome IX (Figure S2B). However, these gene groupings were rarely enriched for particular classes of genes, although they may be

more informative when combined with knowledge of the mutations carried by these strains. We conclude that descendants of disomic strains with improved growth share a gene expression signature.

Identification of Point Mutations Associated with Increased Proliferation Rates in Aneuploid Yeast Cells

Evolved aneuploid strains that proliferate faster yet have maintained both copies of the disomic chromosome probably harbor heritable alterations not detectable by CGH. We selected 14 strains in which to identify these genetic alterations because their proliferation rates were significantly improved compared to the parent strain (Figure 1B). Tiling arrays or deep sequencing identified 43 single-nucleotide polymorphisms (SNPs) that led to nonsynonymous changes (Table 1) and four SNPs that led to synonymous genetic alterations that were verified by Sanger sequencing (Table S4, part A). In two evolved isolates of disome XIII, we could not detect any nonsynonymous genetic changes. A 1 base pair deletion, ten synonymous alterations, and 21 nonsynonymous alterations were present in the parental disomic strains (Table S4, part B). We note that the mutations already present in the parental disomic strains were probably acquired during their construction and could also confer a growth advantage.

Each evolved strain contained between two and seven SNPs, and little overlap was detected among descendants from the same parent strain (Table 1), indicating that different alterations lead to improved proliferation in the different disomic strains. Identical point mutations were only isolated among different descendants of disomes XI and XIV, indicating that a selective sweep had not occurred in the evolution experiments. Interestingly, all three evolved disome XVI strains contained unique mutations in the poorly characterized *SVF1* gene (Table 1). The emergence of mutations in this gene in three independent isolates of disome XVI with improved growth properties suggests that inactivation or hyperactivation of this factor (we do not know how the identified point mutations affect *SVF1* function) confers a selective advantage on strains disomic for chromosome XVI.

Mutations in two genes were identified in descendants of different disomes. Point mutations in the gene encoding the vacuolar-targeting factor Vsp64 were identified in descendants of disome IX and XI (Table 1). Mutations (premature stop codons) in the gene encoding the deubiquitinating enzyme Ubp6 were identified in descendants of disome V and IX. This finding raises the interesting possibility that mutations exist that improve growth rates of more than one disome.

Genes involved in chromatin remodeling, stress response, and protein folding, as well as ribosomal RNA (rRNA) processing, were among those mutated in the evolved disomic strains and could contribute to the improved proliferative abilities of the evolved disomic strains. Striking, however, was the fact that fast growing descendants of strains disomic for chromosomes V, VIII, IX, XI, and XIV harbored mutations in genes encoding proteins involved in proteasomal degradation (*UBP6*, *RPT1*, *RSP5*, *UBR1*). These results suggest that changes in protein degradation lead to an improvement in fitness in multiple aneuploid yeast strains.

Loss of *UBP6* Function Suppresses the Proliferation Defect of Several Disomic Yeast Strains

We decided to test whether a causal relationship exists between mutations in *UBP6* and improved proliferation rates of the evolved strains, because sequence analysis identified premature stop codons in *UBP6* in two different evolved disomic strains. Ubp6 contains an ubiquitin-like (UBL) domain in its N terminus that mediates binding to the proteasome and a peptidase domain in the C-terminal half of the protein (Figure 2A). Strain Dis V-14.1 carries a nonsense mutation resulting in the conversion of glutamic acid 256 to a stop codon (*ubp6E256X*; Figure 2A). Strain Dis IX-14.1 harbors an *UBP6* allele that carries a premature stop codon at position 404 (Figure 2A). Both mutations leave the UBL domain of the protein intact but cause enough of a truncation to inactivate Ubp6's protease activity. To determine whether the expression of this truncated version of *UBP6* was at least in part responsible for the decrease in generation time of strains Dis V-14.1 and Dis IX-14.1, we analyzed disome V cells carrying the *ubp6E256X* mutation.

To assess the effects of this mutation on fitness, we performed a competition assay. In this assay, strains disomic for chromosome V carrying a *GFP-PGK1* fusion integrated at *URA3* were cocultured with disome V cells carrying the *ubp6E256X* mutation also marked with *URA3.* We then monitored the fraction of GFP positive cells in the cultures over time by flow cytometry. Control experiments showed that, with the exception of strains disomic for chromosome XIV, the *GFP-PGK1* fusion did not affect the proliferation rate of the different disomic strains (data not shown).

Disome V cells carrying the *ubp6E256X* mutation proliferated significantly better than disome V cells wild-type for *UBP6* (Figure 2B; Figure S3). A truncation mutation in *UBP6* was also identified in disome IX strains with improved proliferative abilities. In this strain too, replacement of the *UBP6* locus with the *ubp6E256X* allele led to an increase in fitness (Figure 2B; Figure S3). Remarkably, the same allele also led to an increase in proliferation rates in strains disomic for chromosome VIII and XI (Figure 2B). The *ubp6E256X* allele did not improve the proliferative abilities of wild-type cells or of five other disomes (disome I, XII, XIII, XV, XVI) that we analyzed (Figure S3) and had adverse effects only in disome II and disome XIV cells (Figure 2B; Figure S3). Deletion of *UBP6* had similar effects on disomic strains as expression of the *UBP6* truncation. An increase in fitness was observed in coculturing assays and in doubling-time measurements (Figures 2C and 2D; Figure S4; data not shown). Analysis of cell-cycle progression of disome V and disome XI cells lacking *UBP6* revealed that the deletion suppresses the G1 delay of these two disomic strains (Figure S1A). Finally, we found that inactivation of *UBP6* led to an increase in fitness of strains disomic for chromosome XI, and V in YEPD medium but not of strains disomic for chromosome VIII or IX (Figure 2E). We conclude that inactivation of *UBP6* improves the growth rates of four different disomic strains in the presence of the translation inhibitor and proteotoxic compound G418. In two disomic strains, growth improvement was also seen in the absence of the drug. Inactivation of *UBP6* did not significantly influence the growth of otherwise wild-type cells in YEPD (Figure 2E) or −His+G418 (Figure 2C; Figures S3 and S4).

Table 1. Nonsynonymous Genetic Changes in the Evolved Disomic Strains

Strain[a]	Gene	Mutation	Method[b]	Protein Function
Dis V-14.1	SNT1	L431R	S, T	Subunit of the Set3C deacetylase complex
Dis V-14.1	RAD3 (het)	D148N	S, T	5′ to 3′ DNA helicase, involved in nucleotide excision repair
Dis V-14.1	UBP6[c]	E256X	S, T	Ubiquitin-specific protease
Dis V-14.1	DYN1	L526R	S	Cytoplasmic dynein heavy chain
Dis V-14.1	TSL1	N127D	S	Subunit of trehalose 6-phosphate synthase
Dis V-14.1	Chr X, 31906	C to G	S, T	Intergenic region
Dis V-14.1	Chr XIII, 442441	A to C	S, T	Intergenic region
Dis VIII-14.1	RPT1	Q281K	T	ATPase part of the 19S regulatory particle of the proteasome
Dis VIII-14.1	Chr V, 140399	C to G	T	Intergenic region
Dis IX-14.1	VPS64[c]	Q23X	T	Vacuole targeting factor
Dis IX-14.1	UBP6[c]	E404X	T	Ubiquitin-specific protease
Dis XI-9.1	VPS64[c]	E103G	S	Vacuole targeting factor
Dis XI-9.1	SRC1	I721V	S	Inner nuclear membrane protein
Dis XI-9.1	Chr IX, 338123	C to T	S	Intergenic region
Dis XI-9.1	Chr XIII, 818616	G to T	S	Intergenic region
Dis XI-9.2	SAS10	G311V	S	Subunit of processome complex
Dis XI-9.2	RSP5[d]	V591M	S, T	Ubiquitin-protein ligase
Dis XI-9.2	Chr IX, 183614[d]	G to A	S, T	Intergenic region
Dis XI-14.1	RSP5[d]	V591M	S, T	Ubiquitin-protein ligase
Dis XI-14.1	Chr IX, 183614[d]	G to A	S, T	Intergenic region
Dis XIV-9.1	YGR266W	D450Y	S	Protein of unknown function
Dis XIV-9.1	Chr VII, 827547	C to T	S	Intergenic region
Dis XIV-9.1	LAG2[d]	D644E	S	Protein involved in determining longevity
Dis XIV-9.1	YNL234W[d]	D16N	S	Heme-binding protein involved in glucose signaling
Dis XIV-9.1	Chr XIV, 623023[d]	C to S	S	Intergenic region
Dis XIV-9.2	UBR1	F951C	S	Ubiquitin-protein ligase
Dis XIV-9.2	DCS2	H269Y	S	Stress induced protein
Dis XIV-9.2	CCT7	P114R	S	Subunit of the chaperonin Cct ring complex
Dis XIV-9.2	Chr XIV, 148095	A to W	S	Intergenic region
Dis XIV-9.2	LAG2[d]	D644E	S	Protein involved in determining of longevity
Dis XIV-9.2	YNL234W[d]	D16N	S	Heme-binding protein involved in glucose signaling
Dis XIV-9.2	Chr XIV, 623023[d]	C to S	S	Intergenic region
Dis XIV-14.2	PRR2	E260X	T	Serine/threonine protein kinase
Dis XIV-14.2	BUD9	E499D	T	Protein involved in bud-site selection
Dis XIV-14.2	Chr XVI, 572683	C to G	T	Intergenic region
Dis XVI-9.1	SAS3	S689R	S	Histone acetyltransferase catalytic subunit of NuA3 complex
Dis XVI-9.1	SVF1[e]	W178X	S	Protein with a potential role in cell survival pathways
Dis XVI-14.1	SEC31	S1116T	S	Essential component of the COPII coat of secretory pathway vesicles
Dis XVI-14.1	UTP10	P173S	S	Subunit of processome complex involved in production of 18S rRNA
Dis XVI-14.1	SVF1[e]	A320P	S	Protein with a potential role in cell survival pathways
Dis XVI-14.2	GRX4	F188L	S	Glutathione-dependent oxidoreductase
Dis XVI-14.2	SVF1[e]	E220X	S	Protein with a potential role in cell survival pathways
Dis XVI-14.2	Chr I, 71729	T to C	S	Intergenic region

[a] 9.1 and 9.2 refer to isolates 1 and 2 from day 9, respectively. 14.1 and 14.2 refer to isolates 1 and 2 from day 14, respectively.
[b] S, solexa sequencing; T, tiling arrays.
[c] This gene is mutated in descendants of different disomes.
[d] This mutation is present in more than one isolate.
[e] Three different mutations of SVF1 are present in three isolates of disome XVI.

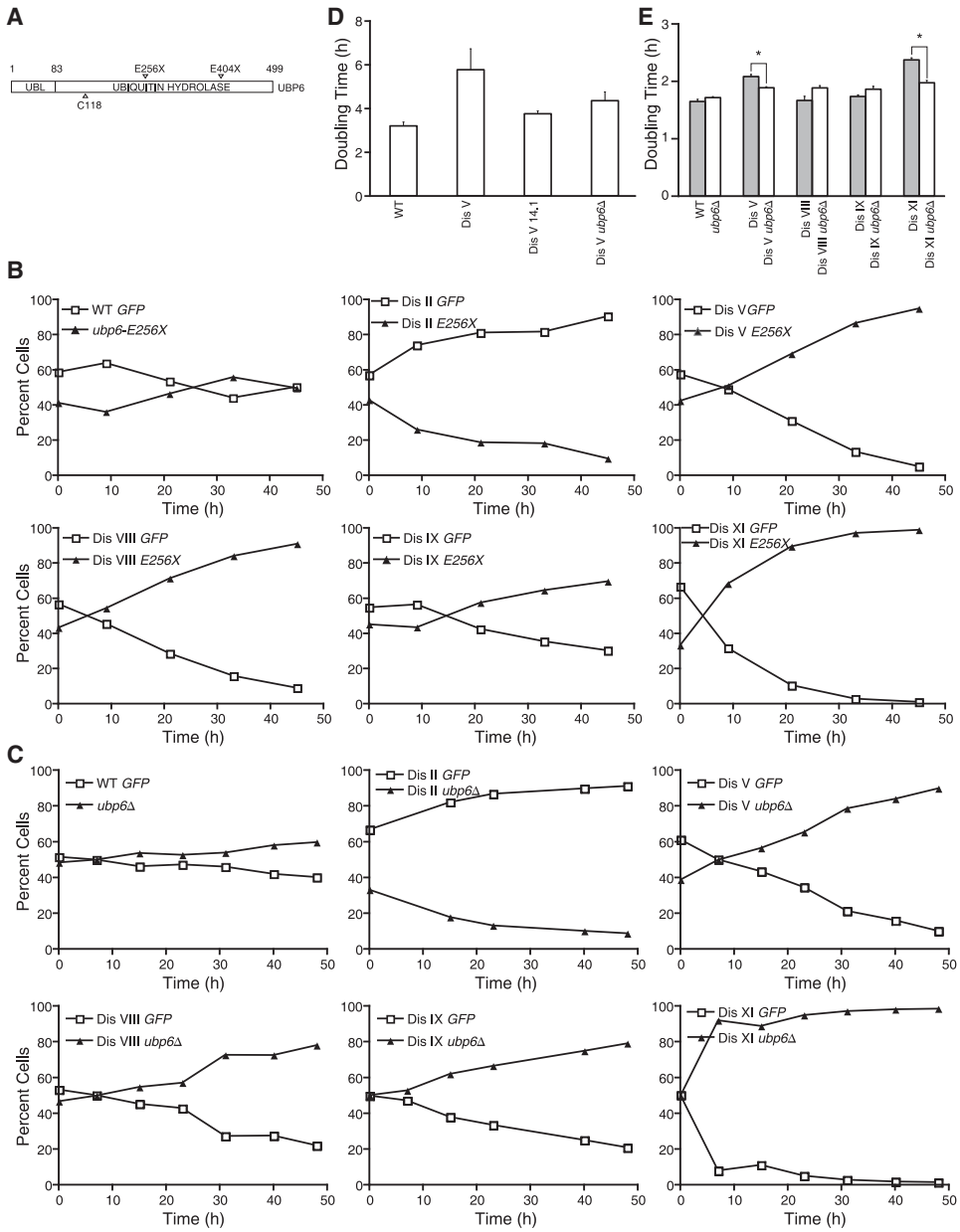

Figure 2. Loss of *UBP6* Function Increases the Fitness of Strains Disomic for Chromosome V, VIII, IX, or XI

(A) Schematic of the Ubp6 domain structure. The N terminus contains an ubiquitin-like domain (UBL, amino acids 1–83), and the C terminus harbors the ubiquitin hydrolase domain (amino acids 83–499). The positions of the catalytic cysteine 118 and the two early stop codons at positions 256 and 404 identified in evolved disome V-14.1 and disome IX-14.1, respectively, are shown.

(B) The percentage of cells in cocultures of strains carrying *PGK1* fused to GFP (open squares) and strains harboring a C-terminal truncated version of *ubp6* (*E256X*, closed triangles) was determined at the indicated times. All strains were grown in −His+G418 medium.

(C) The percentage of cells in cocultures of strains carrying *PGK1* fused to GFP (open squares) and strains harboring a *UBP6* deletion (*ubp6*Δ, closed triangles) was determined at the indicated times. All strains were grown in −His+G418 medium.

(D) Doubling times of the WT, disome V, evolved disome V-14.1, and disome V *ubp6*Δ strains grown in −His+G418 medium (n = 3, error bars represent ± SD).

(E) Doubling times of the WT, disome V, disome VIII, disome IX and disome XI strains either wild-type for *UBP6* or carrying a *UBP6* deletion grown in YEPD medium (n = 3, error bars represent ± SD; *p value < 0.01, Student's t test).

See also Figures S3, S4, and S5.

Next, we wished to determine the degree to which loss of *UBP6* function contributes to the increased fitness of evolved Dis V-14.1 cells. We compared the doubling times of evolved Dis V-14.1 cells with that of disome V cells deleted for *UBP6*. Deletion of *UBP6* did not affect cell-cycle progression or doubling time in wild-type cells (Figure S1A). However, it led to

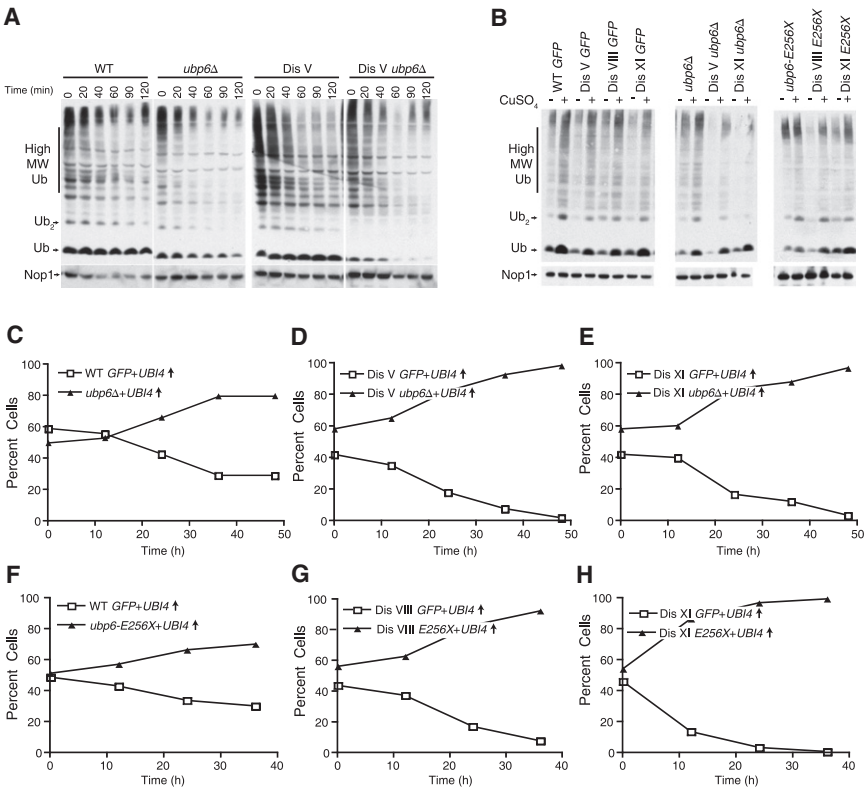

Figure 3. Ubiquitin Depletion Is Not Responsible for the Aneuploidy Tolerance Caused by Loss of *UBP6* Function

(A) Wild-type, *ubp6*Δ, disome V, and disome V *ubp6*Δ cells were grown in −His+G418 medium to an OD_{600} of 1.0 when 100 μg/ml cycloheximide (time = 0 min) was added. Free ubiquitin and ubiquitin conjugates were analyzed by immunoblotting with an anti-ubiquitin antibody at the indicated times.

(B) Ubiquitin levels in the presence (+) or absence (−) of 100 μg/ml $CuSO_4$.

(C– H) The percentage of cells in cocultures of strains carrying *PGK1* fused to GFP (open squares) and strains harboring a *UBP6* deletion (closed triangles) was determined at the indicated times. All strains carry a *CUP1-UBI4* multicopy plasmid whose expression was induced with 100 μg/ml $CuSO_4$. The following strains were compared: wild-type and *UBP6* deletion cells (C), disome V *PGK1-GFP* and disome V *ubp6*Δ cells (D), disome XI *PGK1-GFP* and disome XI *ubp6*Δ (E), wild-type and *ubp6E256X* truncation strains (F), disome VIII *PGK1-GFP* and disome VIII *ubp6E256X* cells, (G) and disome XI *PGK1-GFP* and disome XI *ubp6E256X* cells (H). All strains were grown in −His+G418 medium.

See also Figure S6.

a significant decrease in doubling time in disome V cells (4.2 ± 0.2 hr compared to 5.8 ± 0.8 hr; Figure 2D), but doubling times were not as short as those of the evolved Dis V-14.1 strain (3.8 ± 0.1; Figure 2D). Conversely, restoring *UBP6* function to the evolved Disome V-14.1 isolate reduced the proliferative potential of these cells (Figure S5). We conclude that loss of *UBP6* function contributes to the increased proliferative abilities of Dis V-14.1 cells but other genetic alterations found in this strain also contribute to the increased proliferation rates of this isolate.

Ubiquitin Depletion Is Not Responsible for the Increased Proliferation Rates of Disomic Strains Lacking *UBP6*

Loss of Ubp6 function causes ubiquitin depletion. This leads to cycloheximide sensitivity that can be suppressed by overexpression of ubiquitin (Hanna et al., 2003). Ubiquitin depletion was also observed in disome V *ubp6Δ* cells (Figure 3A). To determine whether ubiquitin depletion was responsible for the increased growth rate of disome V *ubp6Δ* cells, we examined the consequences of increased ubiquitin expression. Disome V and XI cells were cocultured with disome V *ubp6Δ* and disome XI *ubp6Δ* cells, respectively. All strains carried a multicopy plasmid expressing the ubiquitin-encoding gene, *UBI4*, under the control of the copper inducible *CUP1* promoter. Addition of 100 μM $CuSO_4$ significantly increased the steady state levels of free ubiquitin in all strains (Figure 3B). As expected, deletion of *UBP6* suppressed the subtly adverse effects of overexpression of ubiquitin in wild-type cells (Figures 3C and 3F). However, high levels of ubiquitin did not abolish the growth rate improvements of disomic strains brought about by the inactivation of *UBP6* (Figures 3D and 3E; Figure S6A). Similar results were obtained in disome VIII or XI strains harboring the *ubp6E256X* truncation allele (Figures 3G and 3H; Figure S6B) and in competition experiments where only the *UBP6* deleted strains overexpressed ubiquitin (Figure S6C). Our results indicate that low levels of ubiquitin are not responsible for the improved fitness of disomic strains lacking *UBP6*.

Aneuploid Yeast Cells Show an Increased Reliance on Proteasomal Degradation for Survival

Ubp6 deubiquitinates substrates at the proteasome. This activity serves two purposes: recycling of ubiquitin and rescue of proteasome substrates from degradation. *UBP6* antagonizes the proteasome not only through its deubiquitinating activity but also through a noncatalytic mechanism (Hanna et al., 2006; Peth et al., 2009). To determine whether the catalytic or noncatalytic function of Ubp6 was involved in modulating the fitness of disomic yeast strains, we examined the consequences of replacing the catalytic cysteine 110 with alanine (*ubp6CA*). Expression of the *ubp6CA* allele did not affect the proliferative abilities of wild-type cells (Figure 4A; Figure S7). In contrast, coculture of disome VIII, IX, and XI cells with disomic cells carrying the *ubp6CA* allele showed that strains harboring the catalytic dead version of the protein quickly outcompete disomes carrying the wild-type *UBP6* allele (Figures 4B–4D). Our results demonstrate that Ubp6's protease activity antagonizes proliferation in several disomic yeast strains.

Inhibition of the catalytic activity of the mammalian homolog of Ubp6, Usp14, leads to accelerated degradation of a number of

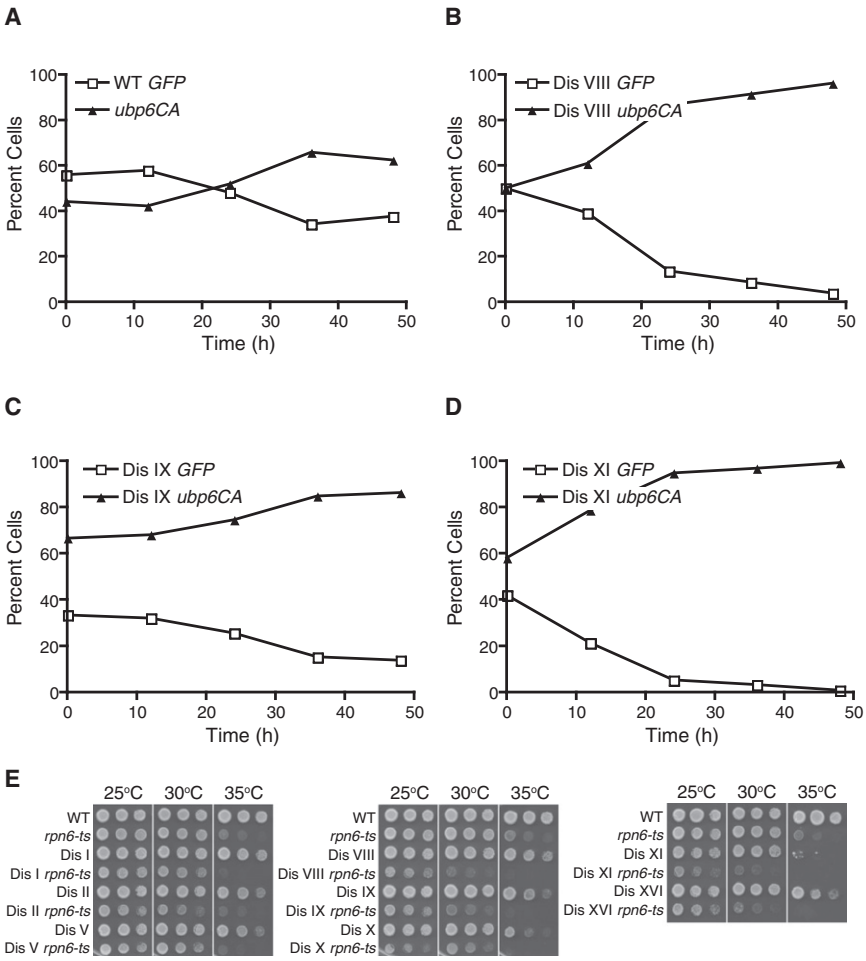

Figure 4. Disomic Strains Exhibit an Increased Reliance on the Proteasome for Survival

(A–D) The percentage of cells in cocultures of strains carrying *PGK1* fused to GFP (open squares) and strains harboring a catalytic dead version of *UBP6* (*ubp6CA*, closed triangles) was determined at the indicated times. The following strains were compared: wild-type and *ubp6CA* cells (A), disome VIII *PGK1-GFP* and disome VIII *upb6CA* cells (B), disome IX *PGK1-GFP* and disome IX *ubp6CA* cells (C), and disome XI *PGK1-GFP* and disome XI *ubp6CA* cells (D). All strains were grown in −His+G418 medium.

(E) Proliferation capabilities of WT, *rpn6-ts*, parental disomes and disomes harboring the *rpn6-ts* allele cells on YEPD medium at 25°C, 30°C, and 35°C; 10-fold serial dilutions are shown. See also Figure S7.

proteins (Lee et al., 2010). These findings lead us to hypothesize that increased proteasomal degradation of an unknown number of proteins improves the fitness of disomic yeast strains. A prediction of this hypothesis is that lowering of proteasomal activity decreases the fitness of disomic yeast strains. This appears to be the case. We previously showed that several disomic strains exhibit increased sensitivity to the proteasome inhibitor MG132 (Torres et al., 2007). Furthermore, a conditional loss-of-function allele in the proteasome lid subunit Rpn6 encoding gene (Ben-Aroya et al., 2008) was synthetic lethal with disomy XII and disomy XIV (data not shown) and decreased the proliferative abilities of almost all disomic strains tested (Figure 4E). Finally, we found that the ubiquitin profile in strains disomic for chromosome V, VIII, or XI resembles that of hypomorphic proteasome mutants: the levels of free ubiquitin are slightly reduced (Figures 3A and 3B). Our results indicate that proteasomal degradation is a rate-limiting pathway in most, or perhaps all, disomic yeast strains.

Consequences of Chromosome V or XIII Disomy on Cellular Protein Composition

To test the idea that increased protein degradation leads to improved fitness of disomic strains, we examined the effects of deletion of *UBP6* on the proteome of a yeast strain whose fitness is improved by the deletion of *UBP6* (disome V) and one that is not (disome XIII). To measure relative protein abundance in disomic and wild-type cells, we utilized stable isotope labeling with amino acids in cell culture (SILAC)-based quantitative mass spectrometry (Extended Experimental Procedures).

SILAC analysis of disome V and XIII relative to wild-type cells revealed quantitative information for 2953 proteins (60.7% of all verified open reading frames [ORFs]) and 3421 proteins (70.3% of all verified ORFs), respectively (Figures 5C and 5E; Table S5). The analysis of the average abundance of proteins encoded by the genes located on chromosome V and XIII demonstrated that the average protein levels of chromosome V-located and chromosome XIII-located genes were increased by 1.8-fold and 1.9-fold compared to the nonchromosome V or XIII encoded proteins, respectively. This correlation is best seen when proteins are sorted with respect to the chromosomal position of their encoding genes (Figures 5C and 5E). To control for artifacts caused by growth in medium containing heavy lysine, we performed a reverse labeling experiment, growing disome V cells in light medium and wild-type cells in heavy medium and compared the results of both analyses. We obtained quantitative information on 2755 proteins, of which 2433 were detected in both forward and reverse experiments (r^2 = 0.59). Of these, 431 proteins show significant up- or downregulation in disome V with high reproducibility (0.49 < $\log_2$ ratio < −0.49; r^2 = 0.78, n = 431; Extended Experimental Procedures).

An interesting additional aspect of the quantitative assessment of the protein composition of the disomic strains is that we are able to determine whether there are proteins whose levels do not increase according to gene copy number. A comprehensive analysis of multiple disomic strains will be presented

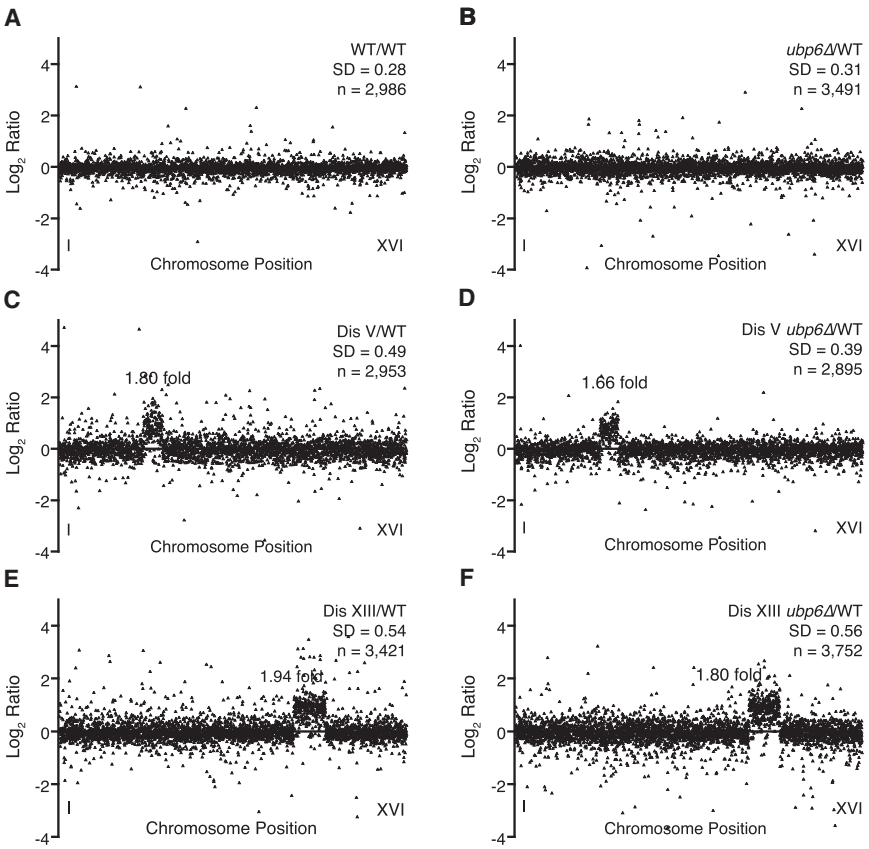

Figure 5. Quantification of the Proteome of Disome V and Disome XIII Strains

The plots show the $\log_2$ ratio of the relative protein abundance compared to wild-type. Protein levels are shown in the order of the chromosomal location of their encoding genes: wild-type/wild-type ratios (A), Δ*ubp6*/wild-type ratios (B), disome V/wild-type ratios (C), disome V Δ*ubp6*/wild-type ratios (D), disome XIII/wild-type ratios (E), and disome XIII Δ*ubp6*/wild-type ratios (F). SD, standard deviation; n, number of proteins quantified. See also the Extended Experimental Procedures. The number in the graphs shows the fold increase in protein levels of proteins encoded by genes located on the disomic chromosome relative to the rest of the proteome.

elsewhere, but several general conclusions are summarized here. We previously analyzed the abundance of a small number of proteins in disomic yeast strains and found that the levels of several of these, especially subunits of macromolecular complexes such as ribosome subunits, did not exhibit a coordinate increase between gene copy number and protein levels (Torres et al., 2007). Consistent with these observations, we find that a considerable fraction of proteins located on chromosome V, 30 of a total 135 proteins detected in both disome V experiments, were not upregulated according to gene copy number. Ninety percent of the proteins that exhibit this property are part of macromolecular complexes. Similar results were obtained with disome XIII cells. Twenty-one percent of proteins (65 of 312) did not show coregulation of protein levels with gene copy number. Sixty-eight percent of these proteins function in large macromolecular complexes. A discrepancy between gene copy number and protein levels was most evident for ribosomal subunits, but was also observed for subunits of ribonucleotide reductase and the vacuolar ATPase. The enrichment of protein complex subunits in the group of disome-encoded proteins that does not show a coordinate upregulation with gene copy number is of high statistical significance, when compared to all proteins encoded by chromosome V or XIII that are part of protein complexes (p value = 1.1×10^{-10} for disome V; p value = 3.8×10^{-3} for disome XIII). Analysis of RNA and protein levels indicates that downregulation of gene expression occurred either at the level of transcription (14 genes in disome V and 22 genes in disome XIII) or posttranscriptionally (16 genes in disome V and 43 genes in disome XIII). Characterization of the feedback mechanisms that ensure accurate stoichiometries of these proteins will be an important aspect of understanding the effects of aneuploidy on cell physiology.

Deletion of *UBP6* Attenuates the Effects of Disomy V on Cellular Protein Composition

Having established the effects of disomy V on the yeast proteome, we next wished to test the hypothesis that loss of *UBP6* function improves the fitness of aneuploid cells such as disome V cells by increasing the degradation of proteins that are in excess in this strain. If this was the case, the protein composition of disome V *ubp6*Δ cells should be more similar to wild-type cells than that of disome V cells is to wild-type cells. This appears to be the case.

We obtained quantitative information on 2895 proteins for disome V *ubp6*Δ cells (Figure 5D; Table S5) and on 3491 proteins for cell lacking *UBP6* (Figure 5B; Table S5). For the analysis of the effects of *UBP6* on protein composition, we only included proteins for which quantitative information was obtained in all four strains (2352 proteins). To determine whether deletion of *UBP6* attenuates the effects of disomy V on the intracellular protein composition, we rank-ordered all of the proteins according to their relative protein abundance levels in the strain disomic for chromosome V and then asked how the expression of these proteins changes in disome V cells lacking *UBP6*. To quantify a potential attenuating effect, we created three bins: one that encompasses all the proteins whose levels fall within one standard deviation (SD) of the distribution (between −0.49 and 0.49, 1947 proteins; Figure 6A), one that encompasses proteins whose relative abundance was low in disome V cells ($\log_2$ ratio < −0.49; 141 proteins Figure 6A), and one that encompasses proteins whose relative abundance was high in the disome V strain ($\log_2$ ratio > 0.49; 264 proteins; Figure 6A). We then calculated the mean of the protein abundance changes for each strain for all three categories and compared them with each other.

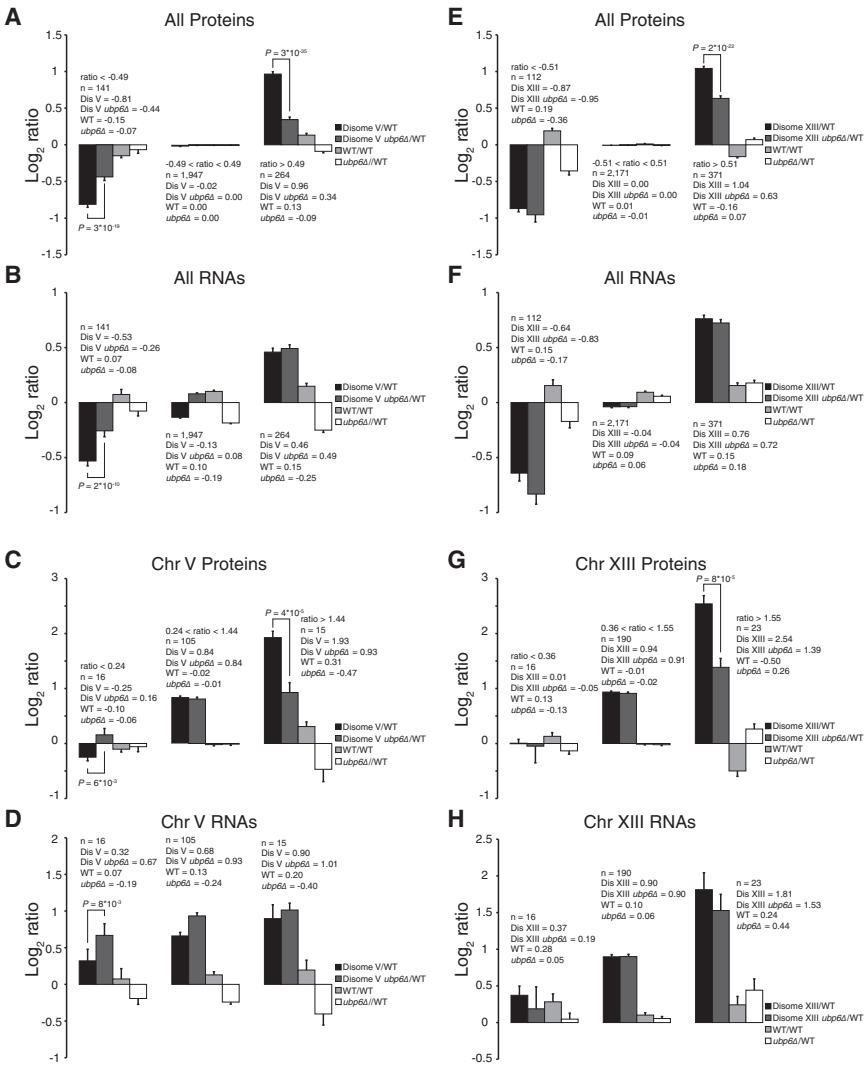

Figure 6. Loss of *UBP6* Function Preferentially Affects Proteins Overproduced in Disome V and Disome XIII Cells Relative to the Wild-Type

(A) Comparison of the means of the $\log_2$ ratios of relative abundance of proteins. Proteins are binned based on their relative levels in disome V cells. Bin 1 (left bars) contains proteins whose levels are lower than one SD of the mean (ratio < −0.49, n = 141). Bin 2 (middle bars) contains proteins whose levels fall within one SD of the mean (−0.49 < ratio < 0.49, n = 1947). Bin 3 (right bars) contains proteins whose levels are greater than one SD (ratio > 0.49, n = 264). Only proteins that were detected in all four experiments were used for this analysis: disome V compared to the wild-type (black bars), disome V *ubp6*Δ compared to the wild-type (dark gray), *ubp6*Δ compared to the wild-type (light gray), and the wild-type/wild-type comparison (white bars) are shown.

(B) RNA levels of the same genes analyzed in (A).

(C) The same analysis as in (A) was performed for proteins encoded by genes located on chromosome V. The SD was that of the distribution of chromosome V-encoded proteins. The bins are as follows: ratio < 0.24, n = 16; 1.44 > ratio > 0.24, n = 105; and ratio > 1.44, n = 15. Nomenclature is as in (A).

(D) RNA levels of the same proteins analyzed in (C).

(E) Comparison of the means of the $\log_2$ ratios of relative abundance of proteins. Proteins are binned based on their relative levels in disome XIII cells as described for disome XIII cells: bin 1 (left bars), ratio < −0.51, n = 112; bin 2 (middle bars), −0.51 < ratio < 0.51, n = 2,171; bin 3 (right bars), ratio > 0.51, n = 371. Only proteins that were detected in all four experiments were used for this analysis: Disome XIII compared to the wild-type (black bars), disome XIII *ubp6*Δ compared to the wild-type (dark gray), *ubp6*Δ compared to the wild-type (light gray), and the wild-type/wild-type comparison (white bars) are shown.

(F) RNA levels of the same proteins analyzed in (E).

(G) The same analysis as in (E) was performed for proteins encoded by genes located on chromosome XIII. The SD was that of the distribution of chromosome XIII encoded proteins. The bins are: ratio < 0.36, n = 16; 1.55 > ratio > 0.36, n = 190; and ratio > 1.55, n = 23. Nomenclature is as in (E).

(H) RNA levels of the same proteins analyzed in (G).

Error bars represent ± standard error of the mean. p, p value paired Student's t test.

The mean of proteins whose levels fall within one SD of the distribution (−0.49 and 0.49) was similar between wild-type, *ubp6Δ*, disome V, and disome V *ubp6Δ* cells (disome V = −0.02; disome V *ubp6Δ* = 0.00; n = 1947; Figure 6A). In contrast, deletion of *UBP6* led to the attenuation in expression levels of proteins whose relative abundances were low ($\log_2$ ratio < −0.49) in disome V cells (disome V = −0.81; disome V *ubp6Δ* = −0.44; p value = 3×10^{-19}; n = 141; Figure 6A). The effects of deletion of *UBP6* were most dramatic among the proteins with the highest relative expression levels in disome V cells (ratio > 0.49). Whereas the mean of this bin was 0.96 for the disome V strain, it was 0.34 for disome V *ubp6Δ* cells (n = 264; p value = 3×10^{-35}; Figure 6A).

The attenuating effects of deletion of *UBP6* were also observed for proteins encoded by genes located on chromosome V, although the effects were not as dramatic, which is most likely due to the limited number of proteins that could be analyzed. The standard deviation we used for this analysis was that of the distribution of proteins located on chromosome V, which was 0.60. The average $\log_2$ expression level of chromosome V proteins was 0.84. The mean of proteins whose levels fall within one SD of the distribution (0.24 and 1.44) was the same between disome V and disome V *ubp6Δ* cells (disome V = 0.84; disome V *ubp6Δ* = 0.84; n = 105; Figure 6C). For proteins with low relative expression levels in disome V cells ($\log_2$ ratios below 0.24), some attenuation was seen as a consequence of *UBP6* deletion (disome V = −0.25; disome V *ubp6Δ* = 0.16; n = 16; p value = 6×10^{-3}; Figure 6C). The attenuation seen for chromosome V proteins with the relative highest levels (ratios above 1.44) was striking. Whereas the mean of this bin was 1.93 for disome V strain, it was 0.93 for disome V *ubp6Δ* cells (n = 15; p value = 4×10^{-5}; Figure 6C).

To determine whether transcriptional or posttranscriptional mechanisms were responsible for the attenuating effects of deletion of *UBP6*, we measured RNA levels in these strains. Microarray analysis showed that deletion of *UBP6* caused an upregulation of transcription of proteins with low relative expression levels in disome V cells (Figure 6B). This finding indicates that transcriptional effects are responsible for the attenuating effects of *UBP6* deletion on proteins underrepresented in disome V cells. In contrast, decreased transcription was not responsible for the attenuating effects of the *UBP6* deletion on proteins with high relative expression levels in disome V cells (Figures 6B and 6D). These data show that inactivating *UBP6* attenuates the effects of disomy V on the proteome in at least two ways: (1) Inactivation of the ubiquitin protease promotes the downregulation of proteins with high relative expression levels in disome V cells by a posttranscriptional mechanism. We presume that increased protein degradation is this mechanism. (2) Deletion of *UBP6* promotes the upregulation of proteins with low relative expression levels in disome V cells by increasing their transcription, most likely by affecting the abundance of proteins that regulate transcription of these genes.

Are the attenuating effects of deleting *UBP6* specific to disome V cells? Deletion of *UBP6* had a similar effect on the proteins with high relative expression levels in disome XIII cells, even though the proteins whose levels are increased in disome XIII cells relative to wild-type are different than in disome V cells (Figures 6E and 6G; p value = 2×10^{-22}). Transcriptional profiling indicated that this attenuating effect occurred at the posttranscriptional level (Figures 6F and 6H). In contrast to disome V cells, deletion of *UBP6* did not increase the abundance of proteins with low relative expression levels in disome XIII cells (Figure 6E).

Our results indicate that deletion of *UBP6* causes attenuation of proteins with high relative expression levels in disomic cells by posttranscriptional mechanisms, most likely by increasing protein degradation. We propose that in disome V cells this effect on the protein composition increases growth rates, because proteins that inhibit proliferation of disome V cells are among the proteins whose levels are lowered by the deletion of *UBP6*. This is not the case in disome XIII cells. We further suggest that the attenuation of low expressed proteins, which occurs in disome V cells but not disome XIII cells, contributes to the differential effect of the *UBP6* deletion on the two disomic strains.

DISCUSSION

Aneuploidy-Tolerating Mutations

This study is to our knowledge the first to describe genetic alterations that allow cells to tolerate the adverse effects of aneuploidy. Our analysis of 13 evolved disomic strains identified gross chromosomal rearrangements, chromosome loss, polyploidization, and point mutations associated with increased proliferation rates. Their characterization revealed a surprising diversity in genetic alterations leading to improved growth rates. We suspect that this is, to some extent, due to the experimental design. The number of evolved strains that we analyzed was small, and clones with improved growth properties were isolated soon after cultures experienced a decrease in doubling time. Nevertheless, it appears that many different types of genetic alterations can lead to improved growth in aneuploid yeast strains. Conversely, most strains appeared to share a common set of gene expression changes, perhaps indicating similar phenotypic consequences.

Although our analysis is far from comprehensive, it was nevertheless striking that different types of genetic alterations predominate in different aneuploid strains. This observation raises the possibility that different disomic yeast strains evolve by different pathways. What determines this difference is not yet clear, but perhaps different forms of genomic instability exist among the disomes that lead to the favoring of one form of evolution over another.

The genetic alterations we identified as causing aneuploidy tolerance fall into two classes: (1) genetic changes unique to a specific isolate or a disomic strain and (2) alterations found in descendants of several disomic strains. Of special interest are genetic alterations that affect the proliferation of multiple aneuploidies. We identified three potential cases: a duplication of 183 kb on chromosome XIII and mutations in *VPS64* and *UBP6*. The *UBP6* mutations indeed led to increased proliferation in four different disomes. It will be interesting to determine whether and how the other genetic alterations affect multiple different disomes.

Modulation of the Ubiquitin-Proteasome Pathway Affects Growth Rates in Aneuploid Yeast Cells

We have demonstrated that inactivation of *UBP6* improves proliferation of strains disomic for chromosome V, VIII, IX, and XI. This effect was especially striking in –His+G418 medium, where we believe the combination of frameshifts induced by G418 and disomy places an especially high burden on the proteasome. How does inactivation of *UBP6* improve the fitness of some aneuploid strains? Our analysis of *UBP6* mutants indicates that Ubp6's proteasome-antagonizing function is responsible for the increase in fitness of the aneuploid strains. Quantitative proteomic approaches further indicate that deletion of *UBP6* reverts the overall protein composition of disome V and XIII cells to a state that is more similar to that of wild-type cells. This appears to be mediated by direct posttranscriptional effects on high abundance proteins in disome V and XIII cells and through indirect transcriptional effect on low-abundance proteins in disome V cells.

Inactivation of *UBP6* attenuates protein levels in both disome V and XIII cells, so why does this improve fitness in disome V but not disome XIII cells? Attenuation of downregulated proteins, which we observe in disome V cells but not disome XIII cells, could be responsible for the differential effects of the *UBP6* deletion. Another not mutually exclusive possibility is that the proteins that antagonize proliferation in disome V cells are more efficiently degraded in the absence of *UBP6* because they are proteasome substrates. In contrast, proteins responsible for decreasing the fitness of disome XIII cells are not. The transcription factor Gcn4 illustrates this point. GO search terminology revealed that genes encoding proteins involved in amino acid metabolism were significantly enriched among the genes most highly expressed in disome V cells and downregulated

when *UBP6* was deleted in these cells (49 out of 175, p value = 3×10^{-33}). Eighty-four of the 175 attenuated genes contain binding sites for the Gcn4 transcription factor in their promoters (http://rsat.ulb.ac.be/rsat/). The *GCN4* gene is located on chromosome V and the levels of the protein are increased in disome V cells. We did not obtain quantitative information on Gcn4 protein levels from disome V *ubp6*Δ cells, but previous work showed that Gcn4 degradation is accelerated in the absence of *UBP6* (Hanna et al., 2006). Deletion of *GCN4* did not improve the fitness of disome V cells (E.T., unpublished data), but scenarios such as the one described for Gcn4 could be the reason for why deletion of *UBP6* affects the growth properties of some aneuploids but not others.

The identification of mutations that accelerate protein degradation as conferring aneuploidy tolerance and the observation that several disomic cells harbored mutations in components of the ubiquitin-proteasome system highlight the importance of ubiquitin-mediated protein degradation in the survival of aneuploid cells. Based on the observations that yeast strains carrying additional yeast chromosomes show synthetic interactions with mutations that affect proteasome function and exhibit an increased sensitivity to conditions that interfere with protein turnover and folding (and strains harboring non-yeast DNA do not), we previously proposed that aneuploid cells are more dependent on these pathways for survival than wild-type cells (Torres et al., 2007). Excess proteins produced by the additional chromosomes place an increased burden on the cell's protein quality control systems. The results presented here support this idea. The quantitative assessment of the cellular protein composition of disome V and XIII cells revealed that the additional chromosomes are indeed producing proteins. Although the proteins that engage the protein degradation and folding machineries will be different for each additional chromosome, the necessity to degrade and fold excess proteins compromises the cell's ability to fold and degrade proteins whose excess presence in the cell interferes with essential cellular processes. Well-known examples of such proteins are α- and β-tubulin (Anders et al., 2009; Katz et al., 1990) and histones (Gunjan and Verreault, 2003; Meeks-Wagner and Hartwell, 1986). We propose that in the absence of *UBP6*, clearance of excess proteins is increased. This improves the fitness of strains, in which the proteasome neutralizes the excess proteins that impair growth. It is important to note that the increased reliance on protein folding and degradation for survival and enhancement of these pathways to improve fitness will not apply to the condition of polyploidy. In polyploid cells, the entire genome is duplicated and protein stoichiometries are not affected.

Aneuploidy-Tolerating Mutations— Implications for Cancer

In humans, more than 90% of all solid tumors are aneuploid. Whether and how aneuploidy promotes tumor formation remains controversial (Holland and Cleveland, 2009; Schvartzman et al., 2010). Irrespective of aneuploidy's role in tumorigenesis, it is clear from our studies that for tumor cells to acquire high proliferative potential and to become malignant, they must overcome the antiproliferative effects associated with aneuploidy. Obtaining a comprehensive list of genes that modulate the fitness of specific aneuploidies or the aneuploid state overall could provide key insights into how cancer cells evolve to escape the adverse effects of aneuploidy. Interestingly, 12 of the 29 genes found mutated in the evolved yeast strains have human homologs, some of which have been found to be upregulated in tumors.

Finally, our results raise the possibility that aneuploid cancers are under profound proteotoxic stress. This increased reliance of aneuploid tumor cells on the ubiquitin-proteasome pathway could provide the framework for the development of new cancer therapeutics with a broad application spectrum and provide the rational for the use of already approved proteasome inhibitors such as Velcade in the treatment of aneuploid tumors in general.

EXPERIMENTAL PROCEDURES

Yeast Strains

All strains are derivatives of W303 (A2587) and are listed in Table S6. The *UBP6* deletion, *UBP6* truncation alleles, and *PGK1-yEGFP-CaURA3* were created with the PCR-based method described in Longtine et al. (1998). The *ubp6C110A* allele was provided by D. Finley. The temperature-sensitive *rpn6-ts* allele is described in Ben-Aroya et al. (2008). Disomy of all strains was confirmed by CGH analysis (Torres et al., 2007) and is available at http://puma.princeton.edu/ and in the Gene Expression Omnibus under accession number GSE20464. Microarray gene expression data are also deposited under this accession number.

Evolution of Aneuploid Yeast Cells

After inoculation from frozen stock directly into selective media, batch cultures of wild-type and disomic strains were kept in exponential phase by manual dilutions twice a day into fresh selective medium (−His+G418) for 14 days at room temperature. Optical densities varied between OD_{600nm} of ∼0.1 and ∼1.0. Doubling times were calculated daily.

Competition Experiments

Approximately equal amounts of cells with and without PGK1-GFP were mixed in selective medium at OD_{600nm} = 0.2 and maintained in exponential growth phase. Relative cell populations in the cultures were measured by flow cytometry as cells containing PGK1-GFP exhibit three orders of magnitude higher green fluorescence than the non-GFP cells.

Solexa Sequencing

DNA libraries were generated with the Illumina DNA preparation kit. A summary of the number of reads, total number of bases sequenced, and coverage are presented in Table S7. We used the assembled genome of S288C (http://downloads.yeastgenome.org/) and aligned our wild-type strain (W303, A2587) sequences with the Maq software package (http://maq.sourceforge.net/). We found 1396 SNPs in W303 compared to S288C. Using the assembled S288C genome and taking into account the SNPs found in W303, we created a reference genome. The methods of SNP identification are described in detail in the Extended Experimental Procedures.

Other techniques are described in the Extended Experimental Procedures.

ACCESSION NUMBERS

The Gene Expression Omnibus accession number for all the microarray data including CGH and gene expression analysis reported in this paper is GSE20464.

SUPPLEMENTAL INFORMATION

Supplemental Information includes Extended Experimental Procedures, seven figures, and seven tables and can be found with this article online at doi:10.1016/j.cell.2010.08.038.

ACKNOWLEDGMENTS

We are grateful to Daniel Finley, Philip Hieter, and Juergen Dohmen for reagents and to Daniel Finley, John Hanna, Frank Solomon, and members of the Amon lab for suggestions and their critical reading of this manuscript. This work was supported by National Institutes of Health grant GM56800 and a Charles King Trust postdoctoral Fellowship to ET. M.J.D. and C.M.T. were supported in part by National Institutes of Health grant P50 GM071508. A.A. is also an Investigator of the Howard Hughes Medical Institute.

Received: February 10, 2010
Revised: June 14, 2010
Accepted: August 3, 2010
Published online: September 16, 2010

REFERENCES

Albertson, D.G., Collins, C., McCormick, F., and Gray, J.W. (2003). Chromosome aberrations in solid tumors. Nat. Genet. *34*, 369–376.

Anders, K.R., Kudrna, J.R., Keller, K.E., Kinghorn, B., Miller, E.M., Pauw, D., Peck, A.T., Shellooe, C.E., and Strong, I.J. (2009). A strategy for constructing aneuploid yeast strains by transient nondisjunction of a target chromosome. BMC Genet. *10*, 36.

Ben-Aroya, S., Coombes, C., Kwok, T., O'Donnell, K.A., Boeke, J.D., and Hieter, P. (2008). Toward a comprehensive temperature-sensitive mutant repository of the essential genes of Saccharomyces cerevisiae. Mol. Cell *30*, 248–258.

Chernova, T.A., Allen, K.D., Wesoloski, L.M., Shanks, J.R., Chernoff, Y.O., and Wilkinson, K.D. (2003). Pleiotropic effects of Ubp6 loss on drug sensitivities and yeast prion are due to depletion of the free ubiquitin pool. J. Biol. Chem. *278*, 52102–52115.

Davies, J., and Davis, B.D. (1968). Misreading of ribonucleic acid code words induced by aminoglycoside antibiotics. The effect of drug concentration. J. Biol. Chem. *243*, 3312–3316.

Davies, J., Gilbert, W., and Gorini, L. (1964). Streptomycin, Suppression, and the Code. Proc. Natl. Acad. Sci. USA *51*, 883–890.

Dettman, J.R., Sirjusingh, C., Kohn, L.M., and Anderson, J.B. (2007). Incipient speciation by divergent adaptation and antagonistic epistasis in yeast. Nature *447*, 585–588.

Gasch, A.P., Spellman, P.T., Kao, C.M., Carmel-Harel, O., Eisen, M.B., Storz, G., Botstein, D., and Brown, P.O. (2000). Genomic expression programs in the response of yeast cells to environmental changes. Mol. Biol. Cell *11*, 4241–4257.

Gresham, D., Desai, M.M., Tucker, C.M., Jenq, H.T., Pai, D.A., Ward, A., DeSevo, C.G., Botstein, D., and Dunham, M.J. (2008). The repertoire and dynamics of evolutionary adaptations to controlled nutrient-limited environments in yeast. PLoS Genet. *4*, e1000303.

Gunjan, A., and Verreault, A. (2003). A Rad53 kinase-dependent surveillance mechanism that regulates histone protein levels in S. cerevisiae. Cell *115*, 537–549.

Hanna, J., Leggett, D.S., and Finley, D. (2003). Ubiquitin depletion as a key mediator of toxicity by translational inhibitors. Mol. Cell. Biol. *23*, 9251–9261.

Hanna, J., Hathaway, N.A., Tone, Y., Crosas, B., Elsasser, S., Kirkpatrick, D.S., Leggett, D.S., Gygi, S.P., King, R.W., and Finley, D. (2006). Deubiquitinating enzyme Ubp6 functions noncatalytically to delay proteasomal degradation. Cell *127*, 99–111.

Hassold, T.J., and Jacobs, P.A. (1984). Trisomy in man. Annu. Rev. Genet. *18*, 69–97.

Holland, A.J., and Cleveland, D.W. (2009). Boveri revisited: chromosomal instability, aneuploidy and tumorigenesis. Nat. Rev. Mol. Cell Biol. *10*, 478–487.

Katz, W., Weinstein, B., and Solomon, F. (1990). Regulation of tubulin levels and microtubule assembly in Saccharomyces cerevisiae: consequences of altered tubulin gene copy number. Mol. Cell. Biol. *10*, 5286–5294.

Lee, B., Lee, M., Park, S., Oh, D., Elsasser, S., Chen, P., Gartner, C., Dimova, N., Hanna, J., Gygi, S., et al. (2010). Enhancement of proteasome activity by a small-molecule inhibitor of Usp14. Nature *467*, 179–184.

Longtine, M.S., McKenzie, A., 3rd, Demarini, D.J., Shah, N.G., Wach, A., Brachat, A., Philippsen, P., and Pringle, J.R. (1998). Additional modules for versatile and economical PCR-based gene deletion and modification in Saccharomyces cerevisiae. Yeast *14*, 953–961.

Meeks-Wagner, D., and Hartwell, L.H. (1986). Normal stoichiometry of histone dimer sets is necessary for high fidelity of mitotic chromosome transmission. Cell *44*, 43–52.

Peth, A., Besche, H.C., and Goldberg, A.L. (2009). Ubiquitinated proteins activate the proteasome by binding to Usp14/Ubp6, which causes 20S gate opening. Mol. Cell *36*, 794–804.

Schvartzman, J.M., Sotillo, R., and Benezra, R. (2010). Mitotic chromosomal instability and cancer: mouse modelling of the human disease. Nat. Rev. Cancer *10*, 102–115.

Todaro, G.J., and Green, H. (1963). Quantitative studies of the growth of mouse embryo cells in culture and their development into established lines. J. Cell Biol. *17*, 299–313.

Torres, E.M., Sokolsky, T., Tucker, C.M., Chan, L.Y., Boselli, M., Dunham, M.J., and Amon, A. (2007). Effects of aneuploidy on cellular physiology and cell division in haploid yeast. Science *317*, 916–924.

Torres, E.M., Williams, B.R., and Amon, A. (2008). Aneuploidy: cells losing their balance. Genetics *179*, 737–746.

Varshavsky, A. (2005). Regulated protein degradation. Trends Biochem. Sci. *30*, 283–286.

Verma, R., Aravind, L., Oania, R., McDonald, W.H., Yates, J.R., 3rd, Koonin, E.V., and Deshaies, R.J. (2002). Role of Rpn11 metalloprotease in deubiquitination and degradation by the 26S proteasome. Science *298*, 611–615.

Williams, B.R., and Amon, A. (2009). Aneuploidy: cancer's fatal flaw? Cancer Res. *69*, 5289–5291.

Williams, B.R., Prabhu, V.R., Hunter, K.E., Glazier, C.M., Whittaker, C.A., Housman, D.E., and Amon, A. (2008). Aneuploidy affects proliferation and spontaneous immortalization in mammalian cells. Science *322*, 703–709.

Yao, T., and Cohen, R.E. (2002). A cryptic protease couples deubiquitination and degradation by the proteasome. Nature *419*, 403–407.

Zeyl, C. (2006). Experimental evolution with yeast. FEMS Yeast Res *6*, 685–691.

EXTENDED EXPERIMENTAL PROCEDURES

Rationale for Strain Choices and Strain Information

Figure 1. Evolution of Aneuploid Yeast Strains

Rationale: We constructed 13 of the 16 possible disomic strains (disomes III, VI and VII were either lethal or not constructed for technical reasons; (Torres et al., 2007)). We monitored the growth rates of all 13 disomes over 14 days and isolated 4 individual clones for each disome.

(A) Strains utilized: disome V (A14479), disome VIII (A13628), disome XI (A13771), and wild-type (A11311).

Rationale for strain choices: For clarity only three 3 disomes (disome V, VIII and XI) are shown. The other evolution experiments are described in Table S1.

(B) Strains utilized from left to right, top graph: A11311, A12683, A25034, A25035, A12685, A25036, A25037, A12687, A25038, A25039, A14479, A25040, A25041, A13628, A25042, A25043, A13975, A25044, A25045, A12689, A25046, A25047, A13771, A25048, A25049, A12693, A25050, A25051, A12695, A25052, A25053, A13979, A25054, A25055, A12697, A25056, A25057, A12700, A25058, A25059, bottom graph: A11311, A12683, A25060, A25061, A12685, A25062, A25063, A12687, A25064, A25065, A14479, A25066, A25067, A13628, A25068, A25069, A13975, A25070, A25071, A12689, A25072, A25073, A13771, A25074, A25075, A12693, A25076, A25077, A12695, A25078, A25079, A13979, A25080, A25081, A12697, A25082, A25083, A12700, A25084, A25085.

(C) Strains utilized from left to right: WT (A11311), disome V (A14479), disome V-14.1 (A25066), disome V-14.2 (A25067), disome VIII (A13628), disome VIII-14.1 (A25068), disome IX (A13975), disome IX-14.1 (A25070), disome XI (A13771), disome XI-14.1 (A25074), disome XI-14.1 (A25075), disome XIV (A13979), disome XIV-14.2 (A25081), disome XVI (A12700), disome XVI-14.1 (A25084) and disome XVI-14.2 (A25085).

Rationale for strain choices: we decided to analyze gene expression patterns of evolved strains with significantly improved proliferation rates that maintained the parental karyotype. These strains are: descendants of disome V, VIII, IX, XI, XIV and XVI strains. Descendants of disomes I, II and X do not show significant decreases in doubling times. Isolates from disomes IV, XII, XIII and XV strains had significantly altered karyotypes (see Table S2) and were therefore not included in this analysis.

Figure 2. Loss of UBP6 Function Increases the Fitness of Strains Disomic for Chromosomes V, VIII, IX or XI

(B) Strains utilized: WT *PGK1-GFP* (A21954) and *ubp6E256X* (A22366), disome II *PGK1-GFP* (A21956) and disome II *ubp6E256X* (A22368), disome V *PGK1-GFP* (A21972) and disome V *ubp6E256X* (A22370), disome VIII *PGK1-GFP* (A21959) and disome VIII *ubp6E256X* (A22371), disome IX *PGK1-GFP* (A21960) and disome IX *ubp6E256X* (A22387); and, disome XI *PGK1-GFP* (A21962) and disome XI *ubp6E256X* (A22390).

Rationale for strain choices: We introduced *upb6E256X* allele into 11 of 13 disomes. Several attempts to introduce this allele into disome IV failed. 4 disomes whose fitness is improved by the truncation allele and one disome whose fitness is decreased by this allele are shown in this figure, the other strains are shown in Figure S3.

(C) Strain utilized: *PGK1-GFP* (A21954) and *ubp6*Δ (A22024), disome II *PGK1-GFP* (A21956) and disome II *ubp6*Δ (A22026), disome V *PGK1-GFP* (A21958) and disome V *ubp6*Δ (A22028), disome VIII *PGK1-GFP* (A21959) and disome VIII *ubp6*Δ (A22029), disome IX *PGK1-GFP* (A21960) and disome IX *ubp6*Δ (A22030); and, disome XI *PGK1-GFP* (A21962) and disome XI *ubp6*Δ (A22032).

Rationale for strain choices: We introduced *upb6*Δ allele into 11 out of 13 parental disomes. Several attempts to introduce this allele into disomes IV and XII failed. 4 disomes whose fitness is improved by the deletion allele and one disome whose fitness is decreased by this allele are shown in this figure, the other strains are shown in Figure S4.

(D) Strains utilized: Wild-type (A11311), disome V (A14479), evolved disome V-14.1 (A25066), and disome V *ubp6*Δ (A22028).

(E) Strains utilized: Wild-type (A11311), *ubp6*Δ (A22024), disome V (A14479), disome V *ubp6*Δ (A22028), disome VIII (A13628), disome VIII *ubp6*Δ (A22029), disome IX (A13975), disome IX *ubp6*Δ (A22030), disome XI (A13771) and disome XI *ubp6*Δ (A22032).

Figure 3. Ubiquitin Depletion Is Not Responsible for the Aneuploidy Tolerance Caused by Loss of UBP6 Function

(A) Strains utilized are wild-type (A11311), *ubp6*Δ (A22024), disome V (A14479) and disome V *ubp6*Δ (A22028).

Rationale for strain choices: For space limitations, we decided to highlight the effects of deleting *UBP6* on ubiquitin levels in WT and disome V cells. Similar experiments were performed for several other disomic strains and similar results were observed (data not shown).

(B - H) The following strains were compared: (C), wild-type (A25126) and *ubp6* deletion cells (A25095); (D), disome V *PGK1-GFP* (A25127) and disome V *ubp6*Δ (A25098) cells; (E), disome XI *PGK1-GFP* (A25129) and disome XI *ubp6*Δ (A25101); (F), wild-type (A25126) and *ubp6E256X* truncation strains (A25130); (G), disome VIII *PGK1-GFP* (A25128) and disome VIII *ubp6E256X* (A25131) cells; and (H), disome XI *PGK1-GFP* (A25129) and disome XI *ubp6E256X* (A25136) cells.

Rationale for strain choices: In order to demonstrate that ubiquitin depletion is not responsible for the aneuploidy tolerance caused by loss of *UBP6* function, we chose three of the four strains whose fitness was increased by deleting *UBP6*.

Figure 4. Disomic Strains Exhibit an Increased Reliance on the Proteasome for Survival

(A - D) The following strains were compared: (A), wild-type (A25126) and *ubp6CA* (A26338) cells; (B), disome VIII *PGK1-GFP* (A21959) and disome VIII *upb6CA* (A26340) cells; (C), disome IX *PGK1-GFP* (A21960) and disome IX *ubp6CA* (26341) cells; (D), disome XI *PGK1-GFP* (A21962) and disome XI *ubp6CA* (A26342) cells.

Rationale for strain choices: We chose three of the four disomes whose growth was improved by deleting *UBP6* and one strain that was not rescued (disome XV, Figure S7).

(E) Strains utilized are wild-type (A11311), *rpn6-ts* (A26328), disome I (A12683), disome I *rpn6-ts* (A26329), disome II (A12685), disome II *rpn6-ts* (A26330), disome V (A14479), disome V *rpn6-ts* (A26331), disome VIII (A13628), disome VIII *rpn6-ts* (A26332), disome IX (A13975), disome IX *rpn6-ts* (A26333), disome X (12689), disome X *rpn6-ts* (A26334), disome XI (A13771), disome XI *rpn6-ts* (A26335), disome XVI (A12700) and disome XVI *rpn6-ts* (A26336).

Rationale for strain choices: We introduced the *rpn6-ts* allele into 11 of the 13 disomic strains. Attempts to introduce the *rpn6-ts* allele into disome IV and XIII strains failed.

Figure 5. Quantification of the Proteome of Disome V and Disome XIII Strains

Strains utilized are: wild-type (A11311) in (A); Δ*ubp6* (A22024)/wild-type (A11311) in (B); disome V (A23499)/wild-type (A11311) in (C); disome V Δ*ubp6* (A23489)/wild-type (A11311) in (D); disome XIII (A23495)/wild-type (A11311) in (E); and disome XIII Δ*ubp6* (A23503)/wild-type (A11311) in (F).

Figure 6. Loss of UBP6 Function Preferentially Affects Proteins Overproduced in Disome V and Disome XIII Cells relative to wild-type

Strains utilized are the same as in Figure 5.

Detailed Method Description

Ubiquitin levels were analyzed as described by Hanna *et. al*. (Hanna et al., 2003). Tiling microarrays were performed as described in Gresham *et. al.* (Gresham et al., 2006). Because of the difficulty discerning heterozygous sites using tiling arrays, we generated haploid derivatives carrying one copy of the disomic chromosome for analysis. Data were analyzed using the SNP Scanner. SNPs were confirmed by Sanger sequencing in both the original disomic strains and the evolved strains. Expression microarrays were performed as described in Torres et al. (Torres et al., 2007). Raw data are available at the Princeton University Microarray Database (puma.princeton.edu) and in the Gene Expression Omnibus under accession GSE20464.

Methods of SNP Identification

We utilized the Maq software to align the sequences obtained from the evolved disomes to our reference genome and searched for single nucleotide polymorphisms (SNPs). We ranked all SNP calls found in all 11 sequenced genomes according to consensus quality score, depth, hits per position, and neighbor quality. We first filtered the SNP calls applying a consensus quality score of $\geq$ 20, depth of $\geq$ 2, and neighbor quality score of $\geq$ 62. A total of 732 SNPs passed these cutoffs. When we visually inspected the alignments of the 732 SNPs with the reference genome, it became clear that most of the SNP calls were due to sequencing errors in regions enriched for a given base, poor coverage, and alignments to highly repetitive regions such as Ty elements and telomeric repeats. These SNPs were eliminated. Empirical adjustment of the cutoffs in the Maq software showed that consensus quality sores of $>$ 23, neighbor quality scores of $>$ 26 and hits per position scores of $<$ 2.8 resulted in the identification of 89 SNPs, 63 of which were be verified by visual inspection. All SNPs were verified by Saenger sequencing.

Growth of Cells for SILAC Analysis

Cells were grown overnight at 30°C in selective medium (-Lys-His+G418) in the presence of ''light'' or ''heavy'' lysine (100 μg/ml). Batch cultures were diluted to OD_{600nm} = 0.2 the next day and harvested once they reached an OD_{600nm} = 1.0.

Mass Spectrometry Sample Preparation

Cells were mixed in equal numbers and lysed by bead beating in a buffer containing 8 M urea, 75 mM NaCl, 50 mM Tris-Cl, pH 8.2, and a protease inhibitor cocktail (complete mini, Roche) using three cycles of 90 s separated by three minute incubation on ice. The lysates were cleared of unlysed cells and insoluble material by centrifugation at 14,000 x g for 15 min at 4°C. Protein concentrations were determined by a dye binding assay (Bio-Rad). Disulfide bonds were reduced by adding dithiothreitol (Sigma) to a final concentration of 2.5 mM and incubating at 56°C for 40 min. The extract was allowed to cool to room temperature and the reduced cysteines were alkylated by adding iodoacetamide to 7.5 mM and incubating for 40 min in the dark at room temperature. Alkylation was quenched with an additional 5 mM dithiothreitol. Lysates were diluted 2.5-fold with Tris-HCl, pH 8.8 (25 mM final concentration). Lysyl endopeptidase (lysC, Wako, Richmond, VA) was added to a final concentration of 10 ng/μl and digests were allowed to proceed overnight at room temperature with gentle agitation. Digestion was stopped by the addition of formic acid to a final concentration of 1% and precipitates were removed by centrifugation at 14,000 x g for three minutes. The supernatants were applied to pre-equilibrated Sep- Pak tC18 columns (Waters), and the columns were washed with 1% formic acid. Bound peptides were eluted with 70% acetonitrile (ACN), 1% formic acid (FA) and lyophilized.

Strong Cation Exchange Chromatography

Strong cation exchange (SCX) chromatography was performed as described previously (Villen and Gygi, 2008) with minor changes. Briefly, 0.5 mg of a heavy/light (disomic/wt) peptide mixture was resuspended in 250 μl of SCX buffer A (7 mM KH_2PO_4, pH 2.65, 30% ACN) and separated on a 4.6 mm x 200 mm polysulfethyl aspartamide column (5 μm particles; 200 Å pores; PolyLC), using a 36 min gradient from 0% to 50% buffer B (7 mM KH_2PO_4, pH 2.65, 30% ACN, 350 mM KCl) at a flow rate of 1 ml/min. Fractions were

collected every 1.5 min, dried in a speed-vac evaporator (ThermoFisher), resuspended in 1% FA, and desalted using self-packed C18 STAGE-tips (Rappsilber et al., 2003). Peptides were eluted into glass inserts and resuspended in 100 μl of 5% FA.

LC-MS/MS Analysis

One to two μl of each SCX fraction was analyzed by LC-MS/MS on a LTQ-Orbitrap or LTQ-Orbitrap Discovery hybrid linear ion trap (ThermoFisher) using a 125 min method. Between 20 and 22 fractions were analyzed for each experiment. Peptides were introduced into the mass spectrometer by nano-electrospray as they eluted off a self-packed 18 cm, 125 μm (ID) reverse-phase column (packed with 5 μm, 200 Å pores, Magic C18AQ resin, MichromBioResources, Auburn, CA). We used a 95 min gradient of 5%–27% buffer B (97% ACN, 0.125% FA) with an in-column flow rate of 0.5–1.0 μl/minute. For each scan cycle, one high mass resolution full MS scan was acquired in the Orbitrap mass analyzer and up to 10 parent ions were chosen based on their intensity for collision induced dissociation (CID) and MS/MS fragment ion scans at low mass resolution in the linear ion trap. Dynamic exclusion was enabled to exclude ions that had already been selected for MS/MS in the previous 60 s. Ions with a charge of +1 and those whose charge state could not be assigned were also excluded. All scans (MS and MS/MS) were collected in centroid mode.

Database Searching and Filtering

MS/MS spectra were matched to peptide sequences using SEQUEST (Eng et al., 1994) and a composite database containing the translated sequences of all predicted open reading frames of *Saccharomyces cerevisiae* (http://downloads.yeastgenome.org/sequence/genomic_sequence/orf_protein/orf_trans.fasta.gz) and its reversed complement. Search parameters allowed for two missed cleavages, a mass tolerance of 25 ppm, a static modification of 57.02146 Da (carboxyamidomethylation) on cysteine, and dynamic modifications of 15.99491 Da (oxidation) on methionine and 8.01420 Da on lysine. Search results were filtered to a 1% peptide false discovery rate by restricting the mass tolerance window, and setting thresholds for Xcorr and dCn. Further filtering based on the quality of quantitative measurements (see below) resulted in a final protein false discovery rate (fdr) < 1% for all experiments.

Protein Quantification

Automated peptide quantification was performed using the Vista program (Bakalarski et al., 2008). Briefly, the theoretical mass of both heavy and light variants of each peptide was calculated and used to identify ion peaks in the high mass accuracy precursor scans for each. The intensity of the peaks was used to construct ion chromatograms. Candidate peaks were required to fall within a tolerance window equal to five standard deviations of (usually less than +/−6 ppm) from the calculated mass and were filtered to require the predicted isotopic distribution. For each isotopic variant, the background-subtracted area under the curve was determined as a function of elution time and used to calculate the heavy (disomic) to light (wild-type) abundance ratio. We required a minimum signal to noise (SN) of five for at least one of the heavy:light peptide species in each pair for inclusion in the final dataset. In some cases only the heavy or light version of a peptide was found and a SN ratio only existed for one isotopic peptide species (henceforth referred to as exclusive peptides); e.g., the strains used are auxotrophic for Ade1 but this gene is used as a marker on the disomic chromosome – Ade1 peptides were found exclusively with heavy lysine. For such peptides, the peak SN ratio or its inverse is reported as a proxy for the abundance ratio. Manual inspection of exclusive peptides revealed that they were highly enriched in matches to the decoy database, thus they were subjected to additional and more stringent filtering criteria. We demanded that we identify at least three independently quantified exclusive peptides per protein for the inclusion of any one of them. We also demanded that for proteins for which we obtained non-exclusive quantified peptides that the exclusive peptides made up at least a third of all quantified peptides for their inclusion. The protein false discovery rate for the final quantified data sets was < 1% for all experiments. Protein abundance ratios (H:L) were calculated as the median of all unique peptide measurements for all peptides mapping to each protein. Protein ratios were normalized to account for small variations in cell mixing by recentering the $\log_2$ protein abundance ratio distribution over zero using the assumption that most proteins are present at 1:1 ratio. For disomic strains, proteins coded on the disomic chromosome were excluded from this distribution.

Assessment of the Reproducibility of the Mass Spectrometry Data

Wild-type – wild-type comparison: We determined the ratios for 2,986 yeast proteins. The standard deviation (SD) of 0.28 was calculated using the program PRIZM to fit the data to a Gaussian distribution (Standard error of the fitting was 0.005). This analysis revealed that the ratio of 136 proteins (4.6% of total) to fall outside 2*SD of the distribution. These are the proteins that change in response to isotope labeling, biological variability and/or experimental error. GO term enrichment analysis revealed that proteins involved in small molecule/organic acid/amino acid metabolic processes to be enriched in this group of proteins (61 of 136; p value 3e-16). Exclusion of these proteins from the analysis performed in Figure 6 did not significantly change the averages calculated for disome V, disome V *ubp6*Δ, disome XIII and disome XIII *ubp6*Δ.

Linear regression analysis of the disome V and the disome V reverse experiments shows a linear correlation with an R^2 of 0.6. This poor correlation is due to the large number of proteins whose levels do not change significantly compared to WT (n = 1947). The majority of the ratios of these proteins centers around the zero axis and shows a correlation of $R^2 = 0.4$. The comparison of the reproducibility of proteins whose levels change in disome V cells compared to wild-type is therefore the more significant analysis. We detected 141 and 264 proteins in both disome V experiments whose levels are significantly down and upregulated, respectively

compared to wild-type (Figure 6). Linear regression analysis between the disome V and disome V-reverse analysis of these proteins shows a linear fit with an R^2 of 0.78.

SUPPLEMENTAL REFERENCES

Bakalarski, C.E., Elias, J.E., Villén, J., Haas, W., Gerber, S.A., Everley, P.A., and Gygi, S.P. (2008). The impact of peptide abundance and dynamic range on stable-isotope-based quantitative proteomic analyses. J. Proteome Res. *7*, 4756–4765.

Eng, J.K., McCormack, A.L., and Yates Iii, J.R. (1994). An approach to correlate tandem mass spectral data of peptides with amino acid sequences in a protein database. J. Am. Soc. Mass Spectrom. *5*, 976–989.

Gresham, D., Ruderfer, D.M., Pratt, S.C., Schacherer, J., Dunham, M.J., Botstein, D., and Kruglyak, L. (2006). Genome-wide detection of polymorphisms at nucleotide resolution with a single DNA microarray. Science *311*, 1932–1936.

Hanna, J., Leggett, D.S., and Finley, D. (2003). Ubiquitin depletion as a key mediator of toxicity by translational inhibitors. Mol. Cell. Biol. *23*, 9251–9261.

Rappsilber, J., Ishihama, Y., and Mann, M. (2003). Stop and go extraction tips for matrix-assisted laser desorption/ionization, nanoelectrospray, and LC/MS sample pretreatment in proteomics. Anal. Chem. *75*, 663–670.

Torres, E.M., Sokolsky, T., Tucker, C.M., Chan, L.Y., Boselli, M., Dunham, M.J., and Amon, A. (2007). Effects of aneuploidy on cellular physiology and cell division in haploid yeast. Science *317*, 916–924.

Villén, J., and Gygi, S.P. (2008). The SCX/IMAC enrichment approach for global phosphorylation analysis by mass spectrometry. Nat. Protoc. *3*, 1630–1638.

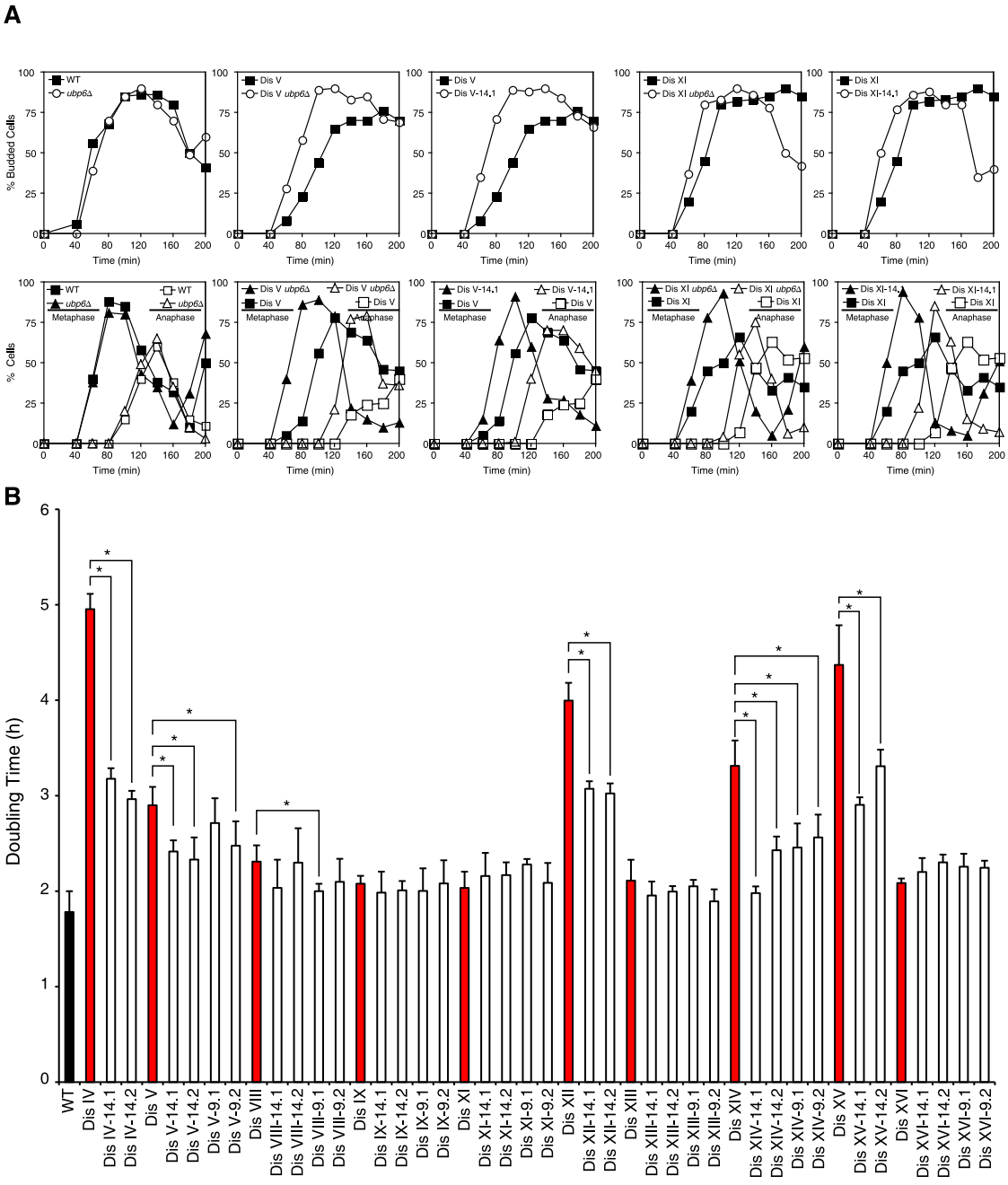

Figure S1. Evolution of Disomic Yeast Strains, Related to Figure 1B

(A) Wild-type (A11311), *ubp6*Δ (A22024), disome V cells (A14479), disome V *ubp6*Δ cells (A22028), disome V-14.1 cells (A25066), disome XI cells (A13771), disome XI *ubp6*Δ (A22032), and disome XI-14.1 cells (A25074) were arrested in G1 with α-factor pheromone in YEPD and released from block into -His +G418 medium. Samples were taken at indicated time points to determine the percent of budded cells (top), and the percent of cells with metaphase (closed symbols) and anaphase (open symbols) spindles (bottom).

(B) Doubling times of continuous cultures in YEPD medium of wild-type (A11311), disome IV (A12687), disome IV-14.1 (A25064), disome IV-14.2 (A25065), disome V (A14479), disome V-14.1 (A25066), disome V-14.2 (A25067), disome V-9.1 (A25040), disome V-9.2 (A25041), disome VIII (A13628), disome VIII-14.1 (A25068), disome VIII-14.2 (A25069), disome VIII-9.1 (A25042), disome VIII-9.2 (A25043), disome IX (A13975), disome IX-14.1 (A25070), disome IX-14.2 (A25071), disome IX-9.1 (A25044), disome IX-9.2 (A25045), disome XI (A13771), disome XI-14.1 (A25074), disome XI-14.2 (A25075), disome XI-9.1 (A25048), disome XI-9.2 (A25049), disome XII (A12693), disome XII-14.1 (A25076), disome XII-14.2 (A25077), disome XIII (A12695), disome XIII-14.1 (A25078), disome XIII-14.2 (A25079), disome XIII-9.1 (A25052), disome XIII-9.2 (A25053), disome XIV (A13979), disome XIV-14.1 (A25080), disome XIV-14.2 (A25081), disome XIV-9.1 (A25054), disome XIV-9.2 (A25055), disome XV (A12697), disome XV-14.1 (A25082), disome XV-14.2 (A25083), disome XVI (A12700), disome XVI-14.1 (A25084), disome XVI-14.2 (A25085), disome XVI-9.1 (A25058), and disome XVI-9.2 (A25059). *p value < 0.01 student's t test.

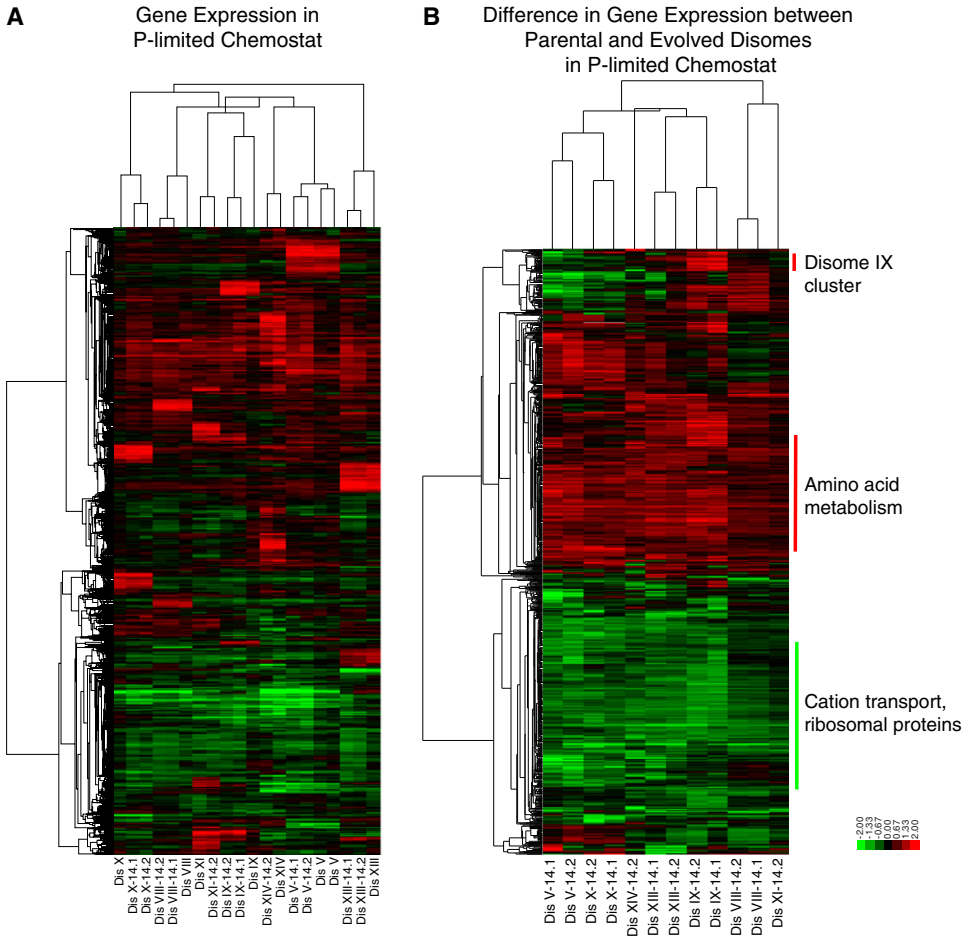

Figure S2. Gene Expression in a Phosphate-Limited Chemostat, Related to Figure 1C

(A) Hierarchically clustered gene expression data obtained from strains grown in the chemostat under phosphate-limiting conditions. Strain order: A12689, A25072, A25073, A25069, A25068, A13628, A13771, A25075, A25071, A25070, A13975, A25081, A13979, A25066, A25067, A14479, A14479, A25078, A25079, A12695.

(B) Hierarchically clustered gene expression data obtained from strains grown in the chemostat under phosphate-limiting conditions. The expression values of the parental disomes were subtracted from the evolved strain data. Red bars indicate putative common transcriptional responses that show upregulation in the evolved disome IX strains only and in all evolved disomic strains analyzed. Green bars indicate a putative common transcriptional responses that show down-regulation in evolved disomic strains (see Table S3 for GO enrichment). Strain order: A25066, A25067, A25073, A25072, A25081, A25078, A25079, A25071, A25070, A25069, A25068, A25075 (each strain is matched to the original disome strain from Torres et al. (Torres et al., 2007)).

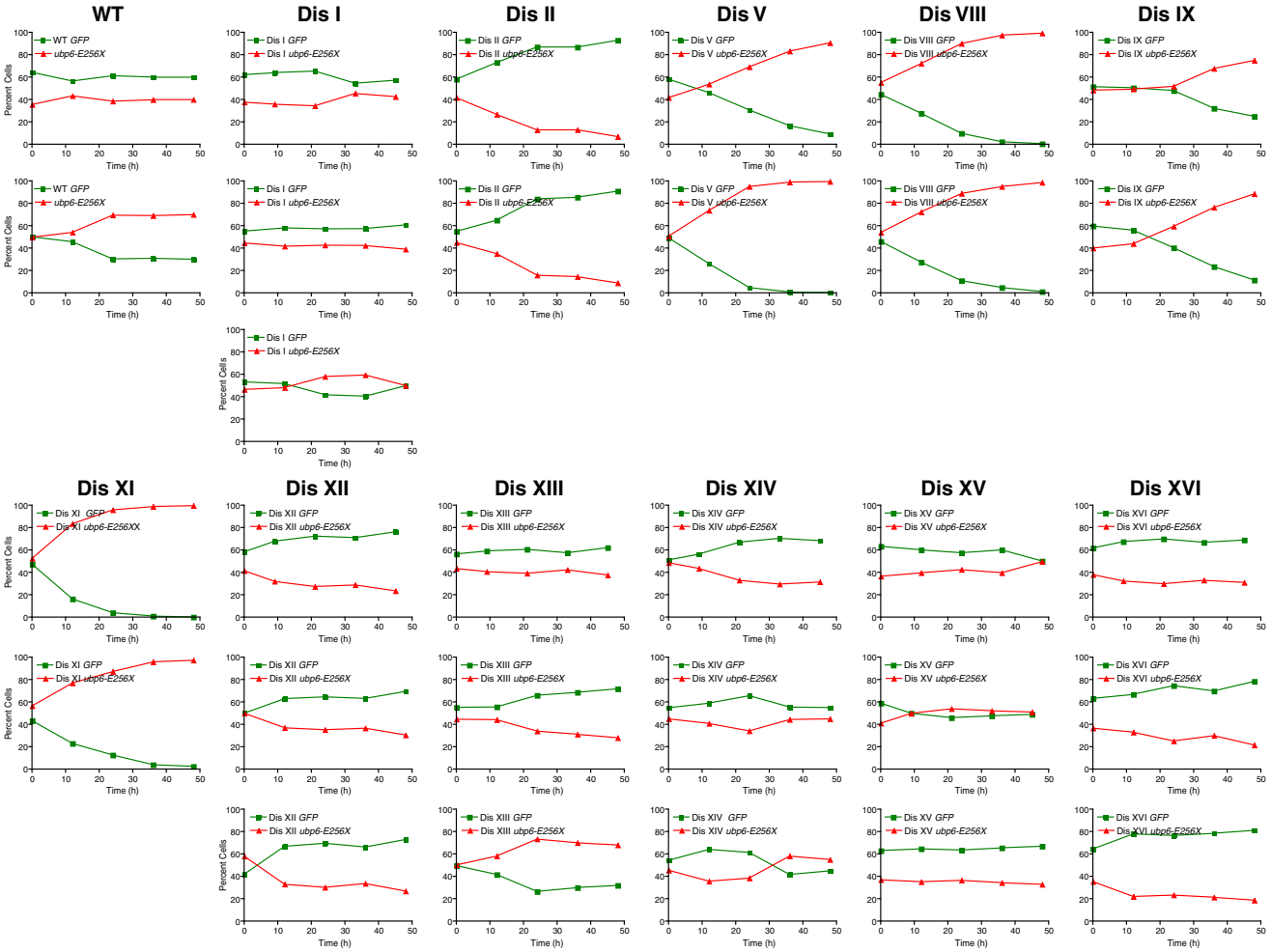

Figure S3. Effects of the *ubp6E256X* Allele on Disomic Strains, Related to Figure 2B

The percentage of cells in co-cultures of strains carrying *PGK1* fused to GFP (green squares) and strains harboring a C-terminal truncated version of *UBP6* (*ubp6E256X*, red triangles) grown in -His+G418 medium was determined at the indicated times. The following strains were compared: WT *PGK1-GFP* (A21954) and *ubp6E256X* (A22366), disome I *PGK1-GFP* (A21955) and disome I *ubp6E256X* (A22367), disome II *PGK1-GFP* (A21956) and disome II *ubp6E256X* (A22368), disome V *PGK1-GFP* (A21972) and disome V *ubp6E256X* (A22370), disome VIII *PGK1-GFP* (A21959) and disome VIII *ubp6E256X* (A22371), disome IX *PGK1-GFP* (A21960) and disome IX *ubp6E256X* (A22387), disome XI *PGK1-GFP* (A21962) and disome XI *ubp6E256X* (A22390), disome XII *PGK1-GFP* (A21963) and disome XII *ubp6E256X* (A22391), disome XIII *PGK1-GFP* (A21964) and disome XIII *ubp6E256X* (A22392), disome XIV *PGK1-GFP* (A21965) and disome XIV *ubp6E256X* (A22393), disome XV *PGK1-GFP* (A21966) and disome XV *ubp6E256X* (A22394); and, disome XVI *PGK1-GFP* (A21967) and disome XVI *ubp6E256X* (A22395).

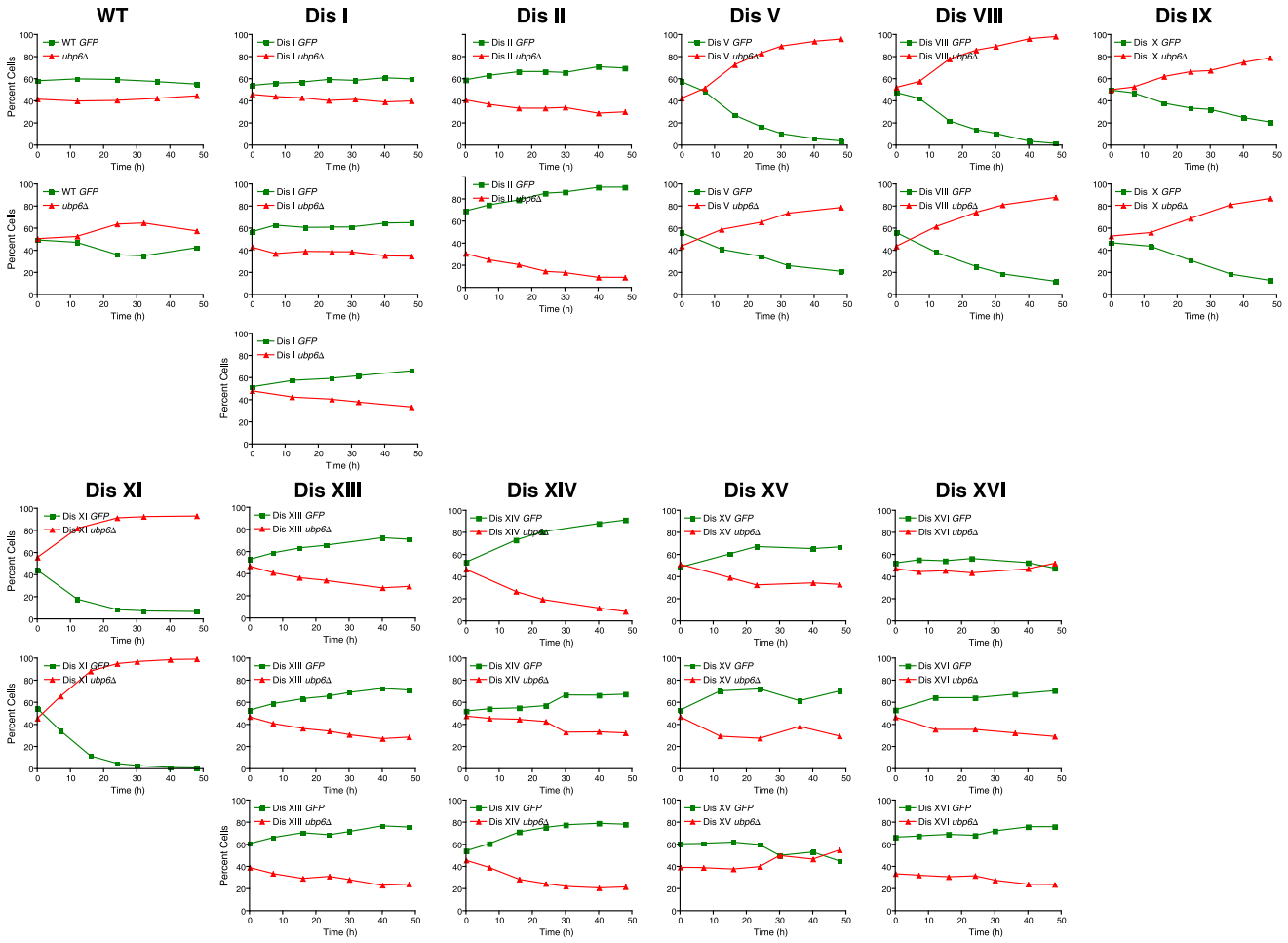

Figure S4. Effects of Deleting *UBP6* on Disomic Strains, Related to Figure 2C

The percentage of cells in co-cultures of strains carrying *PGK1* fused to GFP (green squares) and strains harboring a *UBP6* deletion (*ubp6,*Δ red triangles) grown in -His+G418 medium was determined at the indicated times. The following strains were compared: *PGK1-GFP* (A21954) and *ubp6*Δ (A22024), disome I *PGK1-GFP* (A21955) and disome I Δ*ubp6* (A22025), disome II *PGK1-GFP* (A21956) and disome II *ubp6*Δ (A22026), disome V *PGK1-GFP* (A21958) and disome V *ubp6*Δ (A22028), disome VIII *PGK1-GFP* (A21959) and disome VIII *ubp6*Δ (A22029), disome IX *PGK1-GFP* (A21960) and disome IX *ubp6*Δ (A22030), disome XI *PGK1-GFP* (A21962) and disome XI *ubp6*Δ (A22032), disome XIII *PGK1-GFP* (A21964) and disome XIII *ubp6*Δ (A22034), disome XIV *PGK1-GFP* (A21965) and disome XIV *ubp6*Δ (A22035), disome XV *PGK1-GFP* (A21966) and disome XV *ubp6*Δ (A22036); and, disome XVI *PGK1-GFP* (A21967) and disome XVI *ubp6*Δ (A22037).

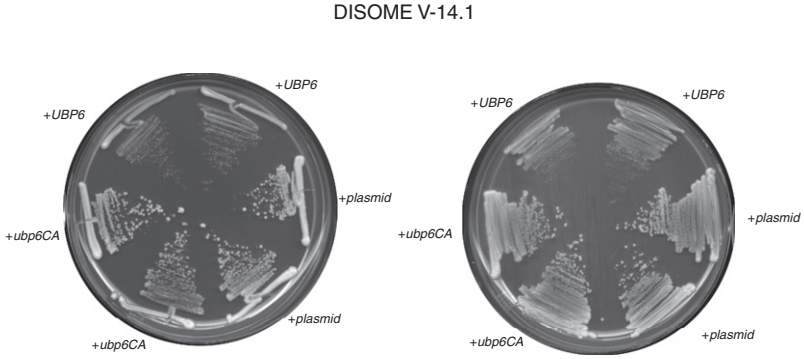

Figure S5. Restoring *UBP6* Function in Disome V 14.1 Cells Impairs Proliferation, Related to Figure 2D

Proliferative capacity of disome V-14.1 cells transformed with either empty plasmid, a plasmid expressing the *UBP6* gene or a catalytic dead version of *UBP6, ubp6CA*. Four independent transformants are shown for each plasmid.

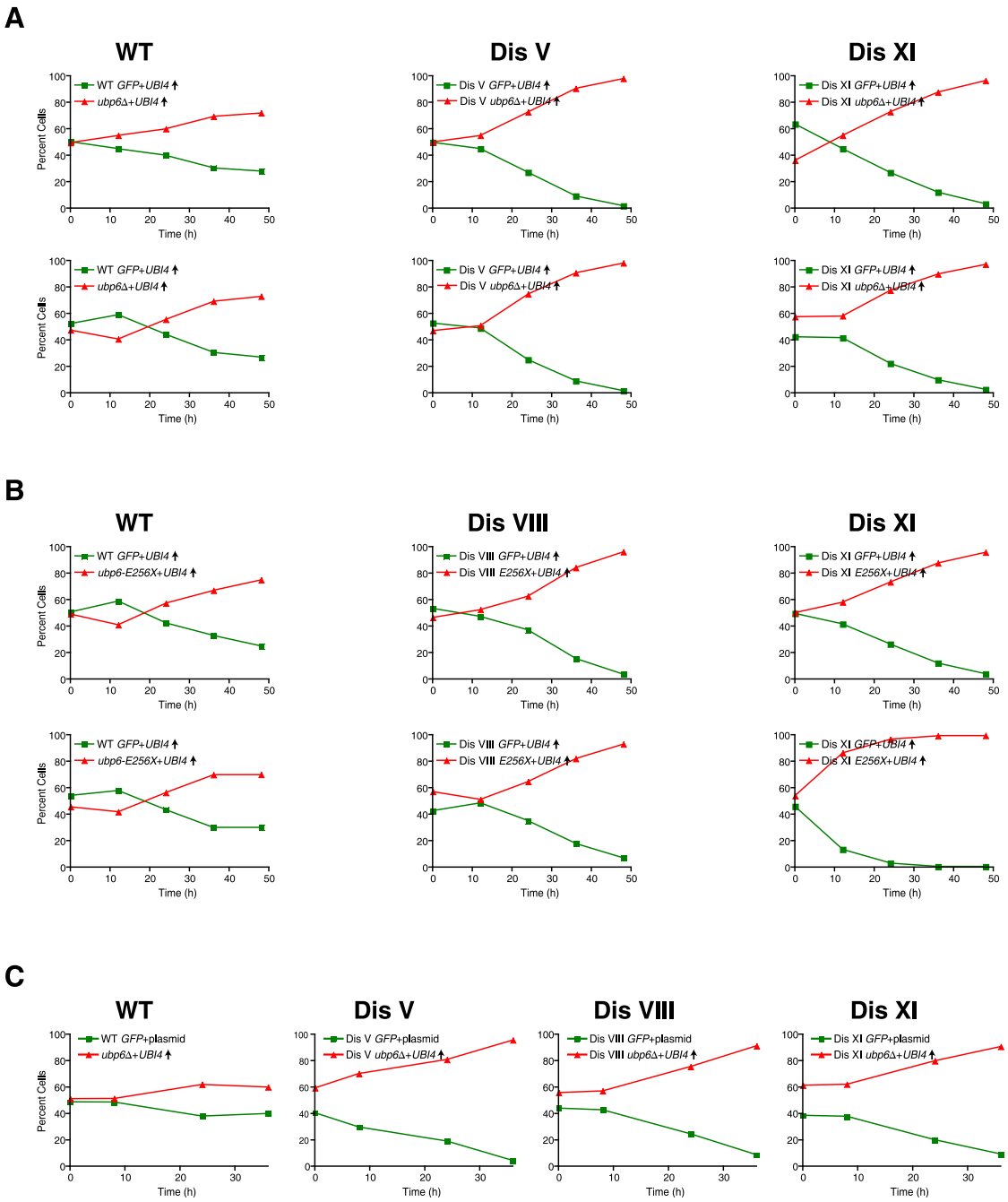

Figure S6. Ubiquitin Depletion Is Not Responsible for the Aneuploidy Tolerance Caused by Loss of *UBP6* Function, Related to Figure 3

(A) The percentage of cells in co-cultures of strains carrying *PGK1* fused to GFP (green squares) and strains harboring a *UBP6* deletion (red triangles) was determined at the indicated times. All strains carry a *CUP1-UBI4* multicopy plasmid whose expression was induced with 100 μg/ml $CuSO_4$. The following strains were compared: wild-type (A25126) and *ubp6* deletion cells (A25095), disome V *PGK1-GFP* (A25127) and disome V *ubp6*Δ (A25098) cells, disome XI *PGK1-GFP* (A25129) and disome XI *ubp6*Δ (A25101).

(B) The percentage of cells in co-cultures of strains carrying *PGK1* fused to GFP (green squares) and strains harboring the *ubp6E256X* truncation (red triangles) was determined at the indicated times. All strains carry a *CUP1-UBI4* multicopy plasmid whose expression was induced with 100 μg/ml $CuSO_4$. The following strains were compared: wild-type (A25126) and *ubp6E256X* truncation strains (A25130), disome VIII *PGK1-GFP* (A25128) and disome VIII *ubp6E256X* (A25131) cells, disome XI *PGK1-GFP* (A25129) and disome XI *ubp6E256X* (A25136) cells.

(C) The percentage of cells in co-cultures of strains carrying *PGK1* fused to GFP (green squares) and strains harboring a *UBP6* deletion (red triangles) was determined at the indicated times. Only *ubp6* deletion cells carry a *CUP1-UBI4* multicopy plasmid whose expression was induced with 100 μg/ml $CuSO_4$. The following

strains were compared: wild-type (A25112) and *ubp6* deletion cells (A25095), disome V *PGK1-GFP* (A25114) and disome V *ubp6*Δ (A25098) cells, disome VIII *PGK1-GFP* (A25115) and disome VIII *ubp6*Δ (A25099) disome XI *PGK1-GFP* (A25117) and disome XI *ubp6*Δ (A25101).

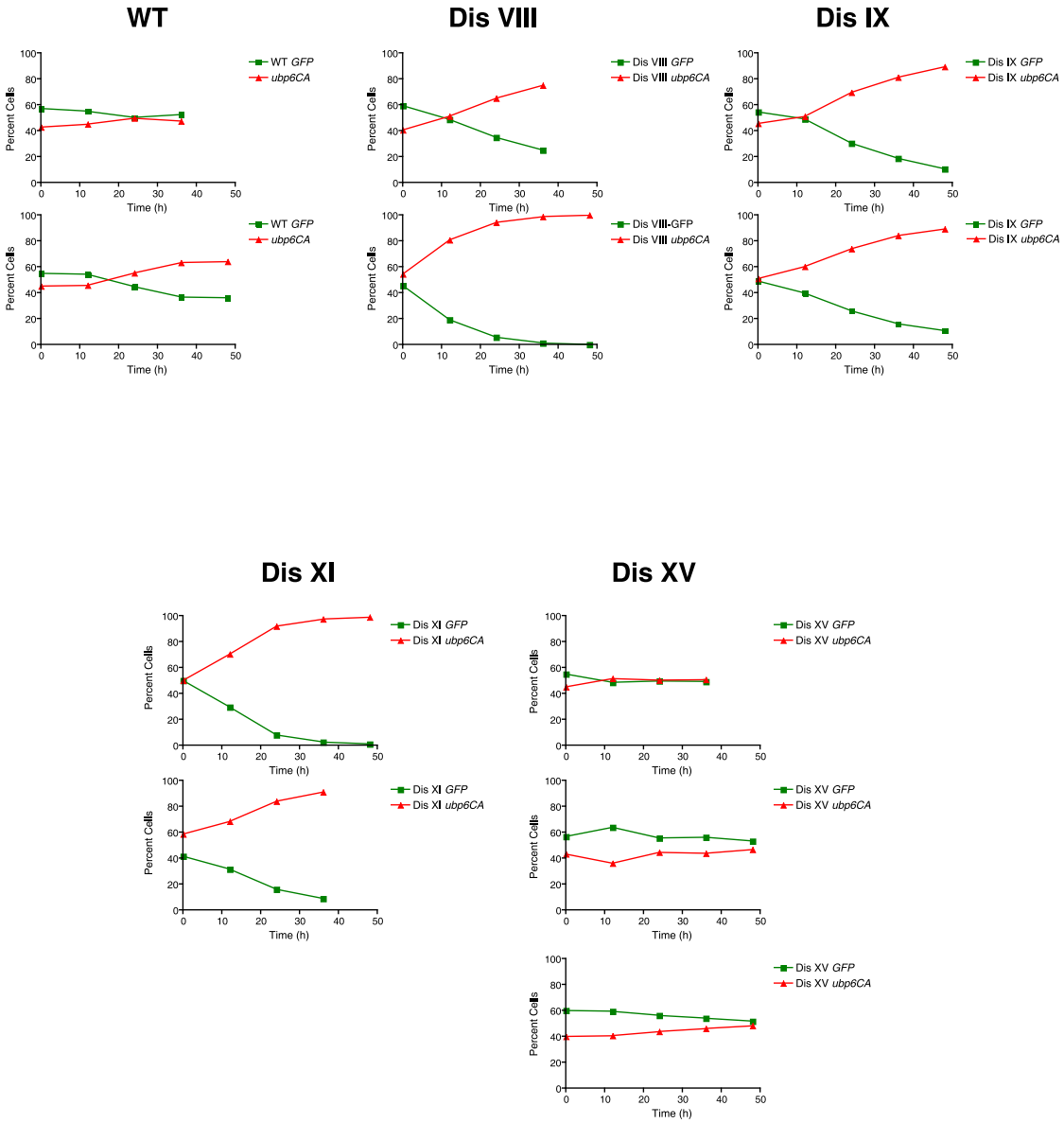

Figure S7. Effects of the *ubp6CA* Allele on Disomes, Related to Figure 4

The percentage of cells in co-cultures of strains carrying *PGK1* fused to GFP (green squares) and strains harboring a catalytic dead version of *UBP6* (*ubp6CA*, red triangles) was determined at the indicated times. The following strains were compared: wild-type (A21954) and *ubp6CA* (A26338) cells, disome VIII *PGK1-GFP* (A21959) and disome VIII *upb6CA* (A26340) cells, disome IX *PGK1-GFP* (A21960) and disome IX *ubp6CA* (26341) cells, disome XI *PGK1-GFP* (A21962) and disome XI *ubp6CA* (A26342) cells, disome XV *PGK1-GFP* (A21965) and disome XV *ubp6CA* (A26344).